Identified Charged Particles and Resonances in Quark and Gluon Jets

P. Abreu, W. Adam, T. Adye, P. Adzic, Z. Albrecht, T. Alderweireld, G D. Alekseev, R. Alemany, T. Allmendinger, P P. Allport, et al.

EUROPEAN ORGANIZATION FOR NUCLEAR RESEARCH

CERN–EP-2000-007

14 January 2000

Identified Charged Particles and Resonances in Quark and Gluon Jets

DELPHI Collaboration

Abstract

A sample of 2.2 million hadronic Z decays, selected from the data recorded by the DELPHI detector at LEP during 1994-1995 was used for an improved measurement of inclusive distributions of π^+ , K^+ and p and their antiparticles in gluon and quark jets. The production spectra of the individual identified particles were found to be softer in gluon jets compared to quark jets, with a higher multiplicity in gluon jets as observed for inclusive charged particles. A significant proton enhancement in gluon jets is observed indicating that baryon production proceeds directly from colour objects. The maxima, ξ^*, of the ξ-distributions for kaons in gluon and quark jets are observed to be different. The study of isoscalar resonance production shows no indication of an excess of $\phi(1020)$ production in gluon jets.

(Submitted to Eur. Phys. J. C)

P.Abreu[22], W.Adam[52], T.Adye[38], P.Adzic[12], Z.Albrecht[18], T.Alderweireld[2], G.D.Alekseev[17], R.Alemany[51], T.Allmendinger[18], P.P.Allport[23], S.Almehed[25], U.Amaldi[9,29], N.Amapane[47], S.Amato[49], E.G.Anassontzis[3], P.Andersson[46], A.Andreazza[9], S.Andringa[22], P.Antilogus[26], W-D.Apel[18], Y.Arnoud[9], B.Åsman[46], J-E.Augustin[26], A.Augustinus[9], P.Baillon[9], A.Ballestrero[47], P.Bambade[20], F.Barao[22], G.Barbiellini[48], R.Barbier[26], D.Y.Bardin[17], G.Barker[18], A.Baroncelli[40], M.Battaglia[16], M.Baubillier[24], K-H.Becks[54], M.Begalli[6], A.Behrmann[54], P.Beilliere[8], Yu.Belokopytov[9], K.Belous[44], N.C.Benekos[33], A.C.Benvenuti[5], C.Berat[15], M.Berggren[24], D.Bertrand[2], M.Besancon[41], M.Bigi[47], M.S.Bilenky[17], M-A.Bizouard[20], D.Bloch[10], H.M.Blom[32], M.Bonesini[29], M.Boonekamp[41], P.S.L.Booth[23], A.W.Borgland[4], G.Borisov[20], C.Bosio[43], O.Botner[50], E.Boudinov[32], B.Bouquet[20], C.Bourdarios[20], T.J.V.Bowcock[23], I.Boyko[17], I.Bozovic[12], M.Bozzo[14], M.Bracko[45], P.Branchini[40], R.A.Brenner[50], P.Bruckman[9], J-M.Brunet[8], L.Bugge[34], T.Buran[34], B.Buschbeck[52], P.Buschmann[54], S.Cabrera[51], M.Caccia[28], M.Calvi[29], T.Camporesi[9], V.Canale[39], F.Carena[9], L.Carroll[23], C.Caso[14], M.V.Castillo Gimenez[51], A.Cattai[9], F.R.Cavallo[5], V.Chabaud[9], M.Chapkin[44], Ph.Charpentier[9], P.Checchia[37], G.A.Chelkov[17], R.Chierici[47], P.Chliapnikov[9,44], P.Chochula[7], V.Chorowicz[26], J.Chudoba[31], K.Cieslik[19], P.Collins[9], R.Contri[14], E.Cortina[51], G.Cosme[20], F.Cossutti[9], H.B.Crawley[1], D.Crennell[38], S.Crepe[15], G.Crosetti[14], J.Cuevas Maestro[35], S.Czellar[16], M.Davenport[9], W.Da Silva[24], G.Della Ricca[48], P.Delpierre[27], N.Demaria[9], A.De Angelis[48], W.De Boer[18], C.De Clercq[2], B.De Lotto[48], A.De Min[37], L.De Paula[49], H.Dijkstra[9], L.Di Ciaccio[9,39], J.Dolbeau[8], K.Doroba[53], M.Dracos[10], J.Drees[54], M.Dris[33], A.Duperrin[26], J-D.Durand[9], G.Eigen[4], T.Ekelof[50], G.Ekspong[46], M.Ellert[50], M.Elsing[9], J-P.Engel[10], M.Espirito Santo[9], G.Fanourakis[12], D.Fassouliotis[12], J.Fayot[24], M.Feindt[18], A.Ferrer[51], E.Ferrer-Ribas[20], F.Ferro[14], S.Fichet[24], A.Firestone[1], U.Flagmeyer[54], H.Foeth[9], E.Fokitis[33], F.Fontanelli[14], B.Franek[38], A.G.Frodesen[4], R.Fruhwirth[52], F.Fulda-Quenzer[20], J.Fuster[51], A.Galloni[23], D.Gamba[47], S.Gamblin[20], M.Gandelman[49], C.Garcia[51], C.Gaspar[9], M.Gaspar[49], U.Gasparini[37], Ph.Gavillet[9], E.N.Gazis[33], D.Gele[10], T.Geralis[12], N.Ghodbane[26], I.Gil[51], F.Glege[54], R.Gokieli[9,53], B.Golob[9,45], G.Gomez-Ceballos[42], P.Goncalves[22], I.Gonzalez Caballero[42], G.Gopal[38], L.Gorn[1], Yu.Gouz[44], V.Gracco[14], J.Grahl[1], E.Graziani[40], P.Gris[41], G.Grosdidier[20], K.Grzelak[53], J.Guy[38], C.Haag[18], F.Hahn[9], S.Hahn[54], S.Haider[9], A.Hallgren[50], K.Hamacher[54], J.Hansen[34], F.J.Harris[36], F.Hauler[18], V.Hedberg[9,25], S.Heising[18], J.J.Hernandez[51], P.Herquet[2], H.Herr[9], T.L.Hessing[36], J.-M.Heuser[54], E.Higon[51], S-O.Holmgren[46], P.J.Holt[36], S.Hoorelbeke[2], M.Houlden[23], J.Hrubec[52], M.Huber[18], K.Huet[2], G.J.Hughes[23], K.Hultqvist[9,46], J.N.Jackson[23], R.Jacobsson[9], P.Jalocha[19], R.Janik[7], Ch.Jarlskog[25], G.Jarlskog[25], P.Jarry[41], B.Jean-Marie[20], D.Jeans[36], E.K.Johansson[46], P.Jonsson[26], C.Joram[9], P.Juillot[10], L.Jungermann[18], F.Kapusta[24], K.Karafasoulis[12], S.Katsanevas[26], E.C.Katsoufis[33], R.Keranen[18], G.Kernel[45], B.P.Kersevan[45], Yu.Khokhlov[44], B.A.Khomenko[17], N.N.Khovanski[17], A.Kiiskinen[16], B.King[23], A.Kinvig[23], N.J.Kjaer[9], O.Klapp[54], H.Klein[9], P.Kluit[32], P.Kokkinias[12], V.Kostioukhine[44], C.Kourkoumelis[3], O.Kouznetsov[17], M.Krammer[52], E.Kriznic[45], Z.Krumstein[17], P.Kubinec[7], J.Kurowska[53], K.Kurvinen[16], J.W.Lamsa[1], D.W.Lane[1], V.Lapin[44], J-P.Laugier[41], R.Lauhakangas[16], G.Leder[52], F.Ledroit[15], V.Lefebure[2], L.Leinonen[46], A.Leisos[12], R.Leitner[31], G.Lenzen[54], V.Lepeltier[20], T.Lesiak[19], M.Lethuillier[41], J.Libby[36], W.Liebig[54], D.Liko[9], A.Lipniacka[9,46], I.Lippi[37], B.Loerstad[25], J.G.Loken[36], J.H.Lopes[49], J.M.Lopez[42], R.Lopez-Fernandez[15], D.Loukas[12], P.Lutz[41], L.Lyons[36], J.MacNaughton[52], J.R.Mahon[6], A.Maio[22], A.Malek[54], T.G.M.Malmgren[46], S.Maltezos[33], V.Malychev[17], F.Mandl[52], J.Marco[42], R.Marco[42], B.Marechal[49], M.Margoni[37], J-C.Marin[9], C.Mariotti[9], A.Markou[12], C.Martinez-Rivero[20], F.Martinez-Vidal[51], S.Marti i Garcia[9], J.Masik[13], N.Mastroyiannopoulos[12], F.Matorras[42], C.Matteuzzi[29], G.Matthiae[39], F.Mazzucato[37], M.Mazzucato[37], M.Mc Cubbin[23], R.Mc Kay[1], R.Mc Nulty[23], G.Mc Pherson[23], C.Meroni[28], W.T.Meyer[1], E.Migliore[9], L.Mirabito[26], W.A.Mitaroff[52], U.Mjoernmark[25], T.Moa[46], M.Moch[18], R.Moeller[30], K.Moenig[9,11], M.R.Monge[14], D.Moraes[49], X.Moreau[24], P.Morettini[14], G.Morton[36], U.Mueller[54], K.Muenich[54], M.Mulders[32], C.Mulet-Marquis[15], R.Muresan[25], W.J.Murray[38], B.Muryn[19], G.Myatt[36], T.Myklebust[34], F.Naraghi[15], M.Nassiakou[12], F.L.Navarria[5], S.Navas[51], K.Nawrocki[53], P.Negri[29], N.Neufeld[9], R.Nicolaidou[41], B.S.Nielsen[30], P.Niezurawski[53], M.Nikolenko[10,17], V.Nomokonov[16], A.Nygren[25], V.Obraztsov[44], A.G.Olshevski[17], A.Onofre[22], R.Orava[16], G.Orazi[10], K.Osterberg[16], A.Ouraou[41], M.Paganoni[29], S.Paiano[5], R.Pain[24], R.Paiva[22], J.Palacios[36], H.Palka[19], Th.D.Papadopoulou[9,33], L.Pape[9], C.Parkes[9], F.Parodi[14], U.Parzefall[23], A.Passeri[40], O.Passon[54], T.Pavel[25], M.Pegoraro[37], L.Peralta[22], M.Pernicka[52], A.Perrotta[5], C.Petridou[48], A.Petrolini[14], H.T.Phillips[38], F.Pierre[41], M.Pimenta[22], E.Piotto[28], T.Podobnik[45], M.E.Pol[6], G.Polok[19], P.Poropat[48], V.Pozdniakov[17], P.Privitera[39], N.Pukhaeva[17], A.Pullia[29], D.Radojicic[36], S.Ragazzi[29], H.Rahmani[33], J.Rames[13], P.N.Ratoff[21], A.L.Read[34], P.Rebecchi[9], N.G.Redaelli[29], M.Regler[52], J.Rehn[18], D.Reid[32], R.Reinhardt[54], P.B.Renton[36], L.K.Resvanis[3], F.Richard[20], J.Ridky[13], G.Rinaudo[47], I.Ripp-Baudot[10], O.Rohne[34], A.Romero[47], P.Ronchese[37], E.I.Rosenberg[1], P.Rosinsky[7], P.Roudeau[20], T.Rovelli[5], Ch.Royon[41], V.Ruhlmann-Kleider[41], A.Ruiz[42], H.Saarikko[16], Y.Sacquin[41], A.Sadovsky[17], G.Sajot[15], J.Salt[51], D.Sampsonidis[12], M.Sannino[14], Ph.Schwemling[24], B.Schwering[54], U.Schwickerath[18], F.Scuri[48], P.Seager[21], Y.Sedykh[17], F.Seemann[54], A.M.Segar[36], N.Seibert[18], R.Sekulin[38], R.C.Shellard[6], M.Siebel[54], L.Simard[41], F.Simonetto[37], A.N.Sisakian[17], G.Smadja[26], O.Smirnova[25], G.R.Smith[38], A.Solovianov[44], A.Sopczak[18], R.Sosnowski[53], T.Spassov[22], E.Spiriti[40], S.Squarcia[14], C.Stanescu[40], S.Stanic[45], M.Stanitzki[18], K.Stevenson[36], A.Stocchi[20], J.Strauss[52], R.Strub[10], B.Stugu[4], M.Szczekowski[53], M.Szeptycka[53], T.Tabarelli[29], A.Taffard[23], O.Tchikilev[44], F.Tegenfeldt[50], F.Terranova[29], J.Thomas[36], J.Timmermans[32], N.Tinti[5], L.G.Tkatchev[17], M.Tobin[23], S.Todorova[9], A.Tomaradze[2], B.Tome[22], A.Tonazzo[9], L.Tortora[40], P.Tortosa[51], G.Transtromer[25], D.Treille[9], G.Tristram[8], M.Trochimczuk[53], C.Troncon[28], M-L.Turluer[41],

I.A.Tyapkin[17], P.Tyapkin[25], S.Tzamarias[12], O.Ullaland[9], V.Uvarov[44], G.Valenti[9,5], E.Vallazza[48], P.Van Dam[32], W.Van den Boeck[2], J.Van Eldik[9,32], A.Van Lysebetten[2], N.van Remortel[2], I.Van Vulpen[32], G.Vegni[28], L.Ventura[37], W.Venus[38,9], F.Verbeure[2], P.Verdier[26], M.Verlato[37], L.S.Vertogradov[17], V.Verzi[28], D.Vilanova[41], L.Vitale[48], E.Vlasov[44], A.S.Vodopyanov[17], G.Voulgaris[3], V.Vrba[13], H.Wahlen[54], C.Walck[46], A.J.Washbrook[23], C.Weiser[9], D.Wicke[54], J.H.Wickens[2], G.R.Wilkinson[36], M.Winter[10], M.Witek[19], G.Wolf[9], J.Yi[1], O.Yushchenko[44], A.Zalewska[19], P.Zalewski[53], D.Zavrtanik[45], E.Zevgolatakos[12], N.I.Zimin[17,25], A.Zintchenko[17], Ph.Zoller[10], G.C.Zucchelli[46], G.Zumerle[37]

[1] Department of Physics and Astronomy, Iowa State University, Ames IA 50011-3160, USA
[2] Physics Department, Univ. Instelling Antwerpen, Universiteitsplein 1, B-2610 Antwerpen, Belgium
and IIHE, ULB-VUB, Pleinlaan 2, B-1050 Brussels, Belgium
and Faculté des Sciences, Univ. de l'Etat Mons, Av. Maistriau 19, B-7000 Mons, Belgium
[3] Physics Laboratory, University of Athens, Solonos Str. 104, GR-10680 Athens, Greece
[4] Department of Physics, University of Bergen, Allégaten 55, NO-5007 Bergen, Norway
[5] Dipartimento di Fisica, Università di Bologna and INFN, Via Irnerio 46, IT-40126 Bologna, Italy
[6] Centro Brasileiro de Pesquisas Físicas, rua Xavier Sigaud 150, BR-22290 Rio de Janeiro, Brazil
and Depto. de Física, Pont. Univ. Católica, C.P. 38071 BR-22453 Rio de Janeiro, Brazil
and Inst. de Física, Univ. Estadual do Rio de Janeiro, rua São Francisco Xavier 524, Rio de Janeiro, Brazil
[7] Comenius University, Faculty of Mathematics and Physics, Mlynska Dolina, SK-84215 Bratislava, Slovakia
[8] Collège de France, Lab. de Physique Corpusculaire, IN2P3-CNRS, FR-75231 Paris Cedex 05, France
[9] CERN, CH-1211 Geneva 23, Switzerland
[10] Institut de Recherches Subatomiques, IN2P3 - CNRS/ULP - BP20, FR-67037 Strasbourg Cedex, France
[11] Now at DESY-Zeuthen, Platanenallee 6, D-15735 Zeuthen, Germany
[12] Institute of Nuclear Physics, N.C.S.R. Demokritos, P.O. Box 60228, GR-15310 Athens, Greece
[13] FZU, Inst. of Phys. of the C.A.S. High Energy Physics Division, Na Slovance 2, CZ-180 40, Praha 8, Czech Republic
[14] Dipartimento di Fisica, Università di Genova and INFN, Via Dodecaneso 33, IT-16146 Genova, Italy
[15] Institut des Sciences Nucléaires, IN2P3-CNRS, Université de Grenoble 1, FR-38026 Grenoble Cedex, France
[16] Helsinki Institute of Physics, HIP, P.O. Box 9, FI-00014 Helsinki, Finland
[17] Joint Institute for Nuclear Research, Dubna, Head Post Office, P.O. Box 79, RU-101 000 Moscow, Russian Federation
[18] Institut für Experimentelle Kernphysik, Universität Karlsruhe, Postfach 6980, DE-76128 Karlsruhe, Germany
[19] Institute of Nuclear Physics and University of Mining and Metalurgy, Ul. Kawiory 26a, PL-30055 Krakow, Poland
[20] Université de Paris-Sud, Lab. de l'Accélérateur Linéaire, IN2P3-CNRS, Bât. 200, FR-91405 Orsay Cedex, France
[21] School of Physics and Chemistry, University of Lancaster, Lancaster LA1 4YB, UK
[22] LIP, IST, FCUL - Av. Elias Garcia, 14-1^{o}, PT-1000 Lisboa Codex, Portugal
[23] Department of Physics, University of Liverpool, P.O. Box 147, Liverpool L69 3BX, UK
[24] LPNHE, IN2P3-CNRS, Univ. Paris VI et VII, Tour 33 (RdC), 4 place Jussieu, FR-75252 Paris Cedex 05, France
[25] Department of Physics, University of Lund, Sölvegatan 14, SE-223 63 Lund, Sweden
[26] Université Claude Bernard de Lyon, IPNL, IN2P3-CNRS, FR-69622 Villeurbanne Cedex, France
[27] Univ. d'Aix - Marseille II - CPP, IN2P3-CNRS, FR-13288 Marseille Cedex 09, France
[28] Dipartimento di Fisica, Università di Milano and INFN-MILANO, Via Celoria 16, IT-20133 Milan, Italy
[29] Dipartimento di Fisica, Univ. di Milano-Bicocca and INFN-MILANO, Piazza delle Scienze 2, IT-20126 Milan, Italy
[30] Niels Bohr Institute, Blegdamsvej 17, DK-2100 Copenhagen Ø, Denmark
[31] IPNP of MFF, Charles Univ., Areal MFF, V Holesovickach 2, CZ-180 00, Praha 8, Czech Republic
[32] NIKHEF, Postbus 41882, NL-1009 DB Amsterdam, The Netherlands
[33] National Technical University, Physics Department, Zografou Campus, GR-15773 Athens, Greece
[34] Physics Department, University of Oslo, Blindern, NO-1000 Oslo 3, Norway
[35] Dpto. Fisica, Univ. Oviedo, Avda. Calvo Sotelo s/n, ES-33007 Oviedo, Spain
[36] Department of Physics, University of Oxford, Keble Road, Oxford OX1 3RH, UK
[37] Dipartimento di Fisica, Università di Padova and INFN, Via Marzolo 8, IT-35131 Padua, Italy
[38] Rutherford Appleton Laboratory, Chilton, Didcot OX11 OQX, UK
[39] Dipartimento di Fisica, Università di Roma II and INFN, Tor Vergata, IT-00173 Rome, Italy
[40] Dipartimento di Fisica, Università di Roma III and INFN, Via della Vasca Navale 84, IT-00146 Rome, Italy
[41] DAPNIA/Service de Physique des Particules, CEA-Saclay, FR-91191 Gif-sur-Yvette Cedex, France
[42] Instituto de Fisica de Cantabria (CSIC-UC), Avda. los Castros s/n, ES-39006 Santander, Spain
[43] Dipartimento di Fisica, Università degli Studi di Roma La Sapienza, Piazzale Aldo Moro 2, IT-00185 Rome, Italy
[44] Inst. for High Energy Physics, Serpukov P.O. Box 35, Protvino, (Moscow Region), Russian Federation
[45] J. Stefan Institute, Jamova 39, SI-1000 Ljubljana, Slovenia and Laboratory for Astroparticle Physics,
Nova Gorica Polytechnic, Kostanjeviska 16a, SI-5000 Nova Gorica, Slovenia,
and Department of Physics, University of Ljubljana, SI-1000 Ljubljana, Slovenia
[46] Fysikum, Stockholm University, Box 6730, SE-113 85 Stockholm, Sweden
[47] Dipartimento di Fisica Sperimentale, Università di Torino and INFN, Via P. Giuria 1, IT-10125 Turin, Italy
[48] Dipartimento di Fisica, Università di Trieste and INFN, Via A. Valerio 2, IT-34127 Trieste, Italy
and Istituto di Fisica, Università di Udine, IT-33100 Udine, Italy
[49] Univ. Federal do Rio de Janeiro, C.P. 68528 Cidade Univ., Ilha do Fundão BR-21945-970 Rio de Janeiro, Brazil
[50] Department of Radiation Sciences, University of Uppsala, P.O. Box 535, SE-751 21 Uppsala, Sweden
[51] IFIC, Valencia-CSIC, and D.F.A.M.N., U. de Valencia, Avda. Dr. Moliner 50, ES-46100 Burjassot (Valencia), Spain
[52] Institut für Hochenergiephysik, Österr. Akad. d. Wissensch., Nikolsdorfergasse 18, AT-1050 Vienna, Austria
[53] Inst. Nuclear Studies and University of Warsaw, Ul. Hoza 69, PL-00681 Warsaw, Poland
[54] Fachbereich Physik, University of Wuppertal, Postfach 100 127, DE-42097 Wuppertal, Germany

1 Introduction

The different colour charge of quarks and gluons leads to specific differences in the particle multiplicity, the energy spectrum and the angular distributions of the corresponding jets. Beyond the study of these differences [1], which are related to the perturbative properties of QCD[1] elementary fields, the comparison of gluon and quark jets opens up the possibility to infer properties of the non-perturbative formation of hadrons directly.

The study of ratios of identified ($\pi^{\pm}, K^{\pm}, p(\bar{p})$) particle distributions in gluon (g) and quark (q) jets is the main subject of this paper. Futhermore the $\phi(1020)$ and the $K^*(892)^0$ production is compared in identified quark and gluon jets.

Gluon jets are selected in $b\bar{b}g$ events by tagging the b quarks using techniques based on the large impact parameters of tracks coming from heavy particle decays. The Ring Imaging Cherenkov Counters (RICH) of the DELPHI detector provide particle identification over a wide momentum range in combination with the ionization loss measurement of the Time Projection Chamber (TPC) and so allow a detailed comparison of identified particle spectra in gluon and quark jets. These are used for a detailed test of QCD based fragmentation models and also to check MLLA[2] and LPHD[3] predictions [2].

This paper is organized as follows. In Section 2 the hadronic event selection, the quark/gluon separation, and the particle identification are described briefly. The experimental results are presented and compared with the predictions of models in Section 3. Finally a summary and the conclusions are presented in Section 4.

2 Experimental Technique and Event Sample

A description of the DELPHI detector, together with a description of its performance, can be found in [3].

2.1 Event Selections

The data collected by DELPHI during 1994-1995 are considered in the present analysis, during which time the RICH [3] detectors (the main particle identification detectors) were fully operational and the Vertex detector was equipped with a three-dimensional readout. The cuts applied to charged and neutral particles and to events in order to select hadronic Z decays are identical to those given in [4] and [5]. The data sample passing the selection of hadronic events contained 1,775,230 events with a small contamination ($< 0.7\%$) arising from $\tau^+\tau^-$ pairs, beam-gas scattering and $\gamma\gamma$ interactions [3].

The influence of the detector performance on the analysis was studied with the full DELPHI simulation program, DELSIM [6]. Events generated with the JETSET 7.3 Parton Shower (PS) model [7], with parameters tuned by DELPHI [8], were passed through DELSIM and processed with the same reconstruction and analysis programs as the real data. Simulations based on the JETSET 7.4 PS model, ARIADNE 4.08 [9], and HERWIG 5.8 [10] with parameters tuned by DELPHI [8] were also used for comparison with the data.

Three-jet events were clustered using the Durham algorithm [11] with a jet resolution parameter $y_{cut} = 0.015$. The value used for the cut-off was optimized using the JETSET

[1] **Q**uantum**C**hromo**D**ynamics
[2] **M**odified **L**eading **L**og **A**pproximation
[3] **L**ocal **P**arton **H**adron **D**uality

7.3 PS model, by maximizing the statistics available and the quark/gluon purity attained for the three-jet event samples [12].

For a detailed comparison of quark and gluon jet properties, it is necessary to obtain samples of quark and gluon jets with similar kinematics and the same underlying scales [13]. To fulfill this condition, two different event topologies were used, as illustrated in FIGURE 1:

- mirror symmetric events, with θ_2 and $\theta_3 \in [150° - 15°, 150° + 15°]$, subsequently called **Y events**, and
- three-fold symmetric events, with θ_2 and $\theta_3 \in [120° - 15°, 120° + 15°]$, subsequently called **Mercedes events**.

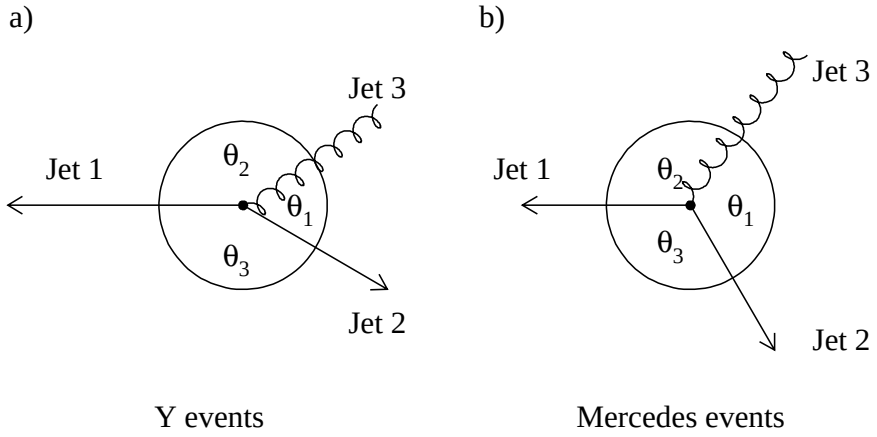

Figure 1: Event topologies of symmetric Y events and Mercedes events; θ_i are the angles between the jets after projection into the event plane.

For Y events only the low energy jets (jets 2 and 3 in FIGURE 1) were used in the analysis. For Mercedes events all jets were used in the analysis.

The jet axes were projected into the event plane, defined as the plane perpendicular to the smallest sphericity eigenvector as obtained from the quadratic momentum tensor, $M_{\alpha\beta} = \sum_{i=1}^{n} p_{i\alpha} p_{i\beta}$. The jets were numbered in decreasing order of jet energy, where the energy of each jet is calculated from the angles between the jets assuming massless kinematics:

$$E_j^{calc} = \frac{\sin\theta_j}{\sin\theta_1 + \sin\theta_2 + \sin\theta_3}\sqrt{s}, \qquad j = 1, 2, 3\,, \tag{1}$$

where θ_j is the interjet angle as defined in FIGURE 1.

In order to enhance the contribution from events with three well-defined jets attributed to $q\bar{q}g$ production, further cuts are applied to the three-jet event samples, as in [4]. The number of three-jet events in the Mercedes and Y samples is 11,685 and 110,628 respectively.

2.2 Quark and Gluon Jet Identification

The identification of gluon jets by anti-tagging of heavy quark jets is identical to that described in [4].

The efficiency and purity calculations were made using events generated by the JETSET 7.3 Monte Carlo model tuned to DELPHI data and passed through DELSIM.

Even in simulated events, the assignment of parton flavours to the jets is not unique, as the decay history is interrupted by the building of strings in models such as JETSET or by the parton assignment of clusters in the case of HERWIG. Thus two independent ways of defining the gluon jet in the fully simulated events were investigated. The first method assumed that the jet which has the largest angle to hadrons containing heavy quarks is the gluon induced jet [4] (angle assignment) and in the second method the jet containing the fewest decay particles from the heavy hadrons was assigned to the gluon (history assignment). Both methods give similar results and therefore the purities can be estimated with small systematic uncertainties.

Gluon jet purities of $\sim 82\%$ for Y events and Mercedes events were achieved. Here the purity is defined as the ratio of real tagged gluons (i.e. jets originating from gluons) to the total number of jets tagged as gluons. There are 24,449 events with an identified gluon jet in the case of Y events and 1,806 in the case of Mercedes events.

2.2.1 Corrections

TABLE 1 shows in detail the fractions in Y events of light ($dusc$) quark, b quark, and gluon jets in the three different jet classes, namely normal mixture jets (i.e. a mixture of quark and gluon jets from events which fail the heavy hadron event tag), b tagged jets and gluon tagged jets.

Jet Class	$dusc$ **quark content**	b **quark content**	**gluon content**
normal mixture	49.5%	1.6%	48.9%
b tagged jets	25.1%	58.2%	16.6%
gluon tagged jets	13.7%	4.2%	82.0%

Table 1: Compositions of different jet classes in Y events. The statistical errors are smaller than 1%.

The use of subtraction techniques which rely only on the knowledge of the proportion of gluon, light, and b quark jets populating the three-jet event samples enables a comparison of pure $dusc$ quark, b quark, and gluon jets.

In the following R_g, R_l and R_b are the distributions of any observable for pure gluon jets, for pure light quark jets, and pure b jets, respectively. Then the measured distributions for jets tagged as gluon jets ($R_{g_{tag}}$) and as b jets ($R_{b_{tag}}$) and in the normal mixture sample (R_{mix}) can be written as follows:

$$\begin{aligned} R_{mix} &= p^l_{mix} \cdot R_l + p^b_{mix} \cdot R_b + p^g_{mix} \cdot R_g \\ R_{b_{tag}} &= p^l_{b_{tag}} \cdot R_l + p^b_{b_{tag}} \cdot R_b + p^g_{b_{tag}} \cdot R_g \\ R_{g_{tag}} &= p^l_{g_{tag}} \cdot R_l + p^b_{g_{tag}} \cdot R_b + p^g_{g_{tag}} \cdot R_g \end{aligned} \qquad (2)$$

where the p^j_i are the corresponding fractions from TABLE 1. For clarity, bin-indices of the distributions R have been omitted in Equation 2. The data distributions for pure b quark, light quark and gluon jets are then obtained by solving Equation 2 for R_b, R_l

[4] There are almost always only two heavy hadrons in an event, because the $g \to q\bar{q}$ splitting into heavy quarks is strongly suppressed.

and R_g [5]. The statistical errors on the fractions p_i^j, which are less than 1%, and their correlations, are fully propagated and included in the errors shown in the following plots and given with the results. This has only a small effect on the total errors.

To correct for the limited detector acceptance, secondary reinteraction of particles, and resolution of the detector, a linear acceptance correction factor

$$C^{acc} = \frac{R^{MC}}{R^{MC+detector}}$$

is also applied to the data in each bin of each distribution. Here R^{MC} denotes the pure model distribution and $R^{MC+detector}$ includes the detector simulation. Long lived particles like the K^0 and Λ^0 were in general considered as instable when computing model distributions.

2.3 Identification of Final State Particles

For the measurement of the π^+ , K^+ and proton content in jets a combined tagging procedure based on the Cherenkov angle measurement in the RICH detector and on the ionization energy loss (dE/dx) in the TPC was applied which is described in detail in [3].

The combined application of TPC and RICH allows a continuous particle identification in the momentum range of 0.3-45.0 GeV/c. TABLE 2 shows which detectors were used to identify pions, kaons, and protons depending on their momentum.

<table>
<tr><th></th><th colspan="7">Momentum Range $[GeV/c]$</th></tr>
<tr><th></th><th>0.3 - 0.7</th><th>0.7 - 0.9</th><th>0.9 - 1.3</th><th>1.3 - 2.7</th><th>2.7 - 9.0</th><th>9.0 -16.0</th><th>16.0 - 45.0</th></tr>
<tr><td>π</td><td>TPC</td><td colspan="3">LRICH S</td><td colspan="3">GRICH S</td></tr>
<tr><td>K</td><td>TPC</td><td colspan="3">LRICH S</td><td>GRICH V
+
LRICH S</td><td colspan="2">GRICH S</td></tr>
<tr><td>p</td><td colspan="2">TPC</td><td>TPC
+
LRICH V</td><td>LRICH S</td><td>GRICH V
+
LRICH S</td><td>GRICH V</td><td>GRICH S</td></tr>
</table>

TPC Identification by measurement of the energy loss
LRICH S(V) Signal (Veto)-Identification with the liquid RICH
GRICH S(V) Signal (Veto)-Identification with the gas RICH

Table 2: Application ranges of the detectors for particle identification

An algorithm was developed to obtain an optimal combination of the particle identification possibilities of the TPC and the RICH. It combines the probabilities for the particle identification with the TPC and the RICH by a simple multiplication and renormalization, and predefines three different identification classes, *loose*, *standard*, and *tight*, by using well chosen cuts on this combined probability distribution. This soft, medium, and hard cuts for the particle identification probabilities allow particle identification performances with different purities R and efficiencies ε:

[5] To obtain a *udscb* reference quark jet sample, Equation 2 has to be modified accordingly.

$$R_i^j = \frac{\#\text{ of particles of kind } i \text{ identified as kind } j}{\#\text{ of all particles of kind } j},$$
$$\varepsilon_i^j = \frac{\#\text{ of particles of kind } i \text{ identified as kind } j}{\#\text{ of all particles of kind } i}.$$

FIGURE 2 shows the efficiency of the combined particle identification of pions, kaons, and protons as a function of the momentum of the particle. The curves of the expected energy loss and the Cherenkov angle,θ_C, are shown in the upper part of FIGURE 2.

FIGURE 3 shows the resulting purities of the particle identification after correction for secondary hadronic interactions with the detector material. It is seen that the purity matrix is predominantly diagonal (FIGURE 3a,f,k). The most important background for the pion reconstruction stems from electrons and muons but is in principle negligible. An exception are energetic electrons and muons from semileptonic hadron decays in b (and c) jets with an identification rate up to 20%. The main background for the kaon selection are pions. A kaon identification purity of $\sim 70\%$ is achieved. Given the very unfavorable production ratio between kaons and pions in hadronic Z decays, this is a very reasonable purity. The lower proton identification purity in b jets is mainly due to the probability to identify kaons as protons because of their higher multiplicity in b jets.

Acceptance correction of the spectra of identified particles

From the measured particle spectra I_π, I_K, and I_p of identified particles one obtains the spectra of pure hadrons S_π, S_K, and S_p by solving the equation system:

$$\begin{pmatrix} I_\pi \\ I_K \\ I_p \end{pmatrix} = \begin{pmatrix} \varepsilon_\pi^\pi & \varepsilon_K^\pi & \varepsilon_p^\pi \\ \varepsilon_\pi^K & \varepsilon_K^K & \varepsilon_p^K \\ \varepsilon_\pi^p & \varepsilon_K^p & \varepsilon_p^p \end{pmatrix} \cdot \begin{pmatrix} S_\pi \\ S_K \\ S_p \end{pmatrix}. \tag{3}$$

This correction is applied before the correction of the purity. The values ε_i^i denote the efficiencies that the particles i are identified correctly; the values ε_i^j with $i \neq j$ are proportional to the background of particle class j.

3 Results

3.1 Identified Particles

Different observables (Z) were measured for identified particles in quark and gluon jets:

- the multiplicity n,
- the momentum p,
- $\xi_p' = -\lg_{10} x_p$ or $\xi_p = -\ln x_p$ (with $x_p = \frac{p_{particle}}{p_{jet}}$) and
- the rapidity $\eta = \ln \frac{E+p_\parallel}{E-p_\parallel}$, with $p_\parallel$ being the corresponding particle momentum along its jet axis.

ξ_p' $(= 1/\ln 10 \cdot \xi_p)$ has been chosen for convenience. Note that the measurement of particle multiplicities of jets is not a well defined subject which depends on details of

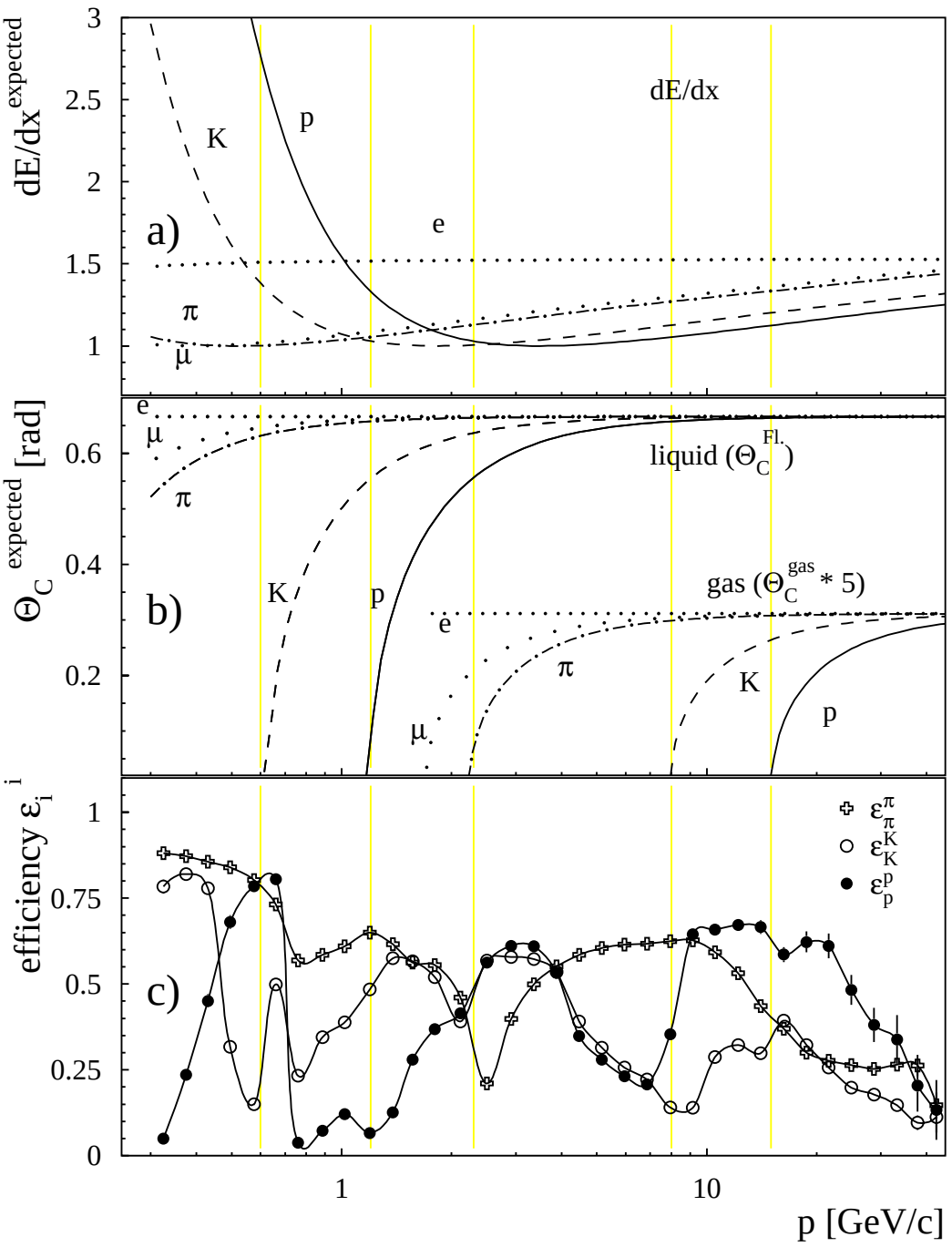

Figure 2: Curves of expected values and efficiencies of the particle identification; a) shows the curve of the expected values for specific ionization for pions (π), kaons (K), protons (p), muons (μ), and electrons (e) as a function of the momentum. b) shows the curve of the expected values for the Cherenkov angle θ_C in the liquid and gas radiator for the same particle hypotheses. ${\theta_C}^{Gas}$ was multiplied by a factor 5. The curves begin at $p = 0.3$GeV/c for the liquid radiator and at 1.7GeV/c for the gas radiator. c) shows the resulting efficiencies for Y events for the standard identification of pions, kaons and protons in the barrel of DELPHI for the 1994-95 data. Vertical lines in all plots indicate the threshold-momenta of π, K and p identification in the two RICH radiators.

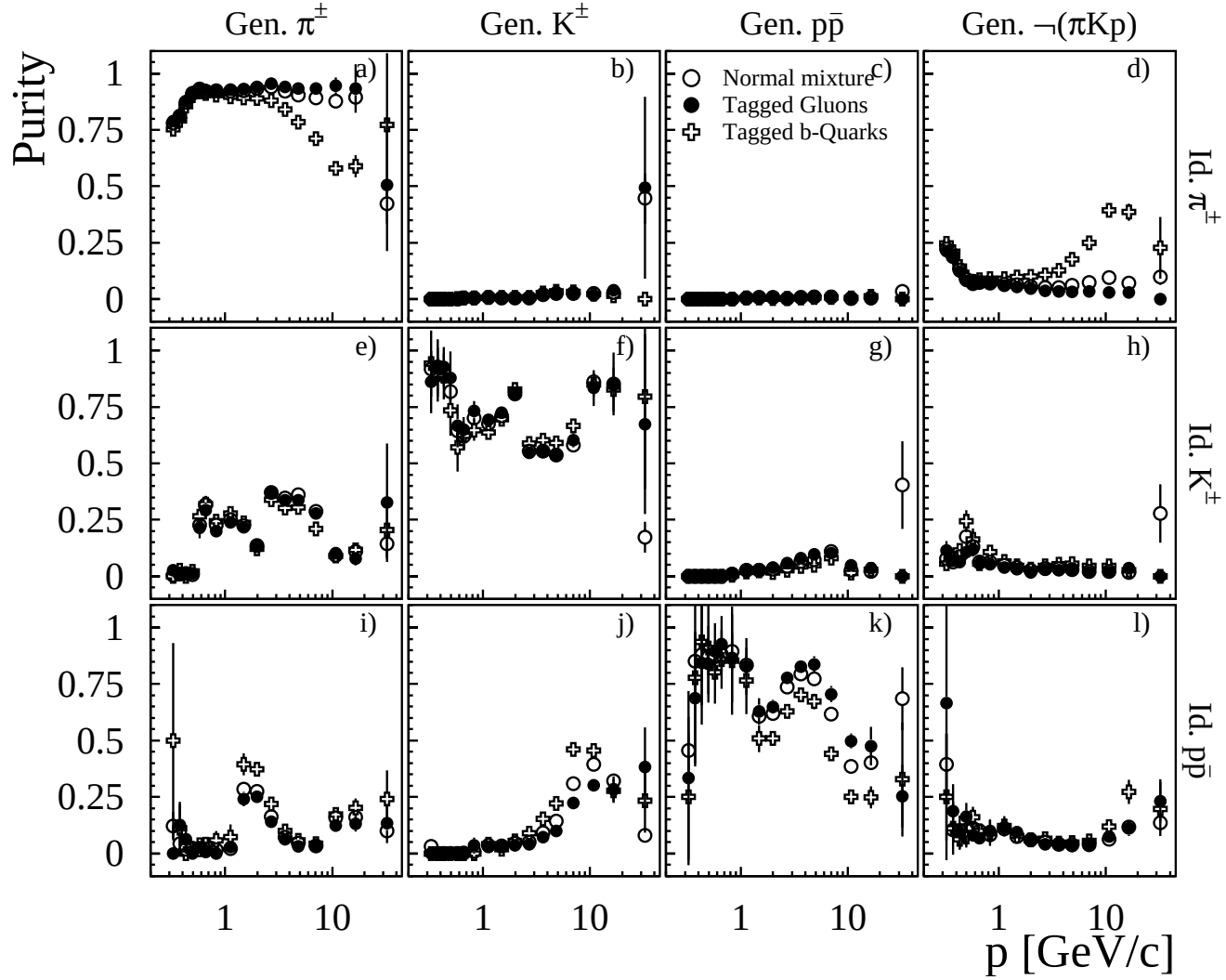

Figure 3: Purity of the particle identification in Y events after correction for secondary interactions. Here 'Gen.' denotes the generated flavour of the particle and 'Id.' denotes the tagged particle flavour.

the jet definition influencing the assignment of low momentum particles to the jets. The given results on multiplicities and also the particle distribution corresponding to very small momenta therefore always refer to the jet definition specified in Section 2.1.

For each observable the following quantities are presented:

- the semi-inclusive spectrum $1/N_{jet}\frac{dn}{dZ}$ for particle X,
- the ratio $R_X(Z)$ of gluon to quark jets for particle X and
- the normalized ratio $R_X^{'}(Z) = R_X(Z)/r_{ch}(Z)$, with $r_{ch}(Z)$ the ratio gluon/quark for all charged particles.

Special emphasis here lies on the measurement of ratios in gluon to quark jets $R_X(Z)$ as in these ratios the systematic error is considerably reduced as most of the systematic uncertainties cancel out. The double ratios $R_X^{'}(Z)$ stress particle specific differences between gluon and quark jets.

In this analysis all quark flavours are considered, i.e. the normal mixture sample here in general also includes identified b events.

3.1.1 Multiplicities

In FIGURE 4 we present the mean multiplicities N_q (N_g) for identified particles in quark and gluon jets respectively, as well as their ratio, $R = N_q/N_g$, and the normalized multiplicity ratios, $R' = R/r_{ch}$.

The multiplicities measured in quark jets for identified hadrons and for all charged hadrons depend on the composition of the quark flavours within the quark jet sample. The quark mixtures dus, $dusc$ and $duscb$ were analysed (see below). The values obtained for the multiplicities N_X^Q and N_X^G and the ratios R_X resp. R'_X are given in TABLE 3. The determination of the systematic errors is described below. In TABLE 4 the normalized multiplicity ratios R'_X are compared to the predictions from the Monte Carlo simulations for Y and Mercedes events. The data show a significant proton enhancement in gluon jets in Y events. A similar enhancement, although less significant, is also seen in Mercedes events. The slight change observed for R'_K and R'_p (see TABLE 3) for different flavour compositions can be understood due to a stronger K production and a depleted proton production in events with heavy quarks.

HERWIG underestimates both the kaon and the proton production in gluon jets. In contrast JETSET and ARIADNE [6] tend to overestimate the proton production in gluon jets. This is less so for the JETSET model with default baryon production. The difference to the other model is that here the extra suppression at the string end, which was introduced to better describe baryon production at large scaled momenta [8], is inactive. The excess of baryon production in gluon jets indicates that baryons are directly produced from a colour string and not via intermediate colour and baryon number neutral clusters. This is discussed in more detail in Section 3.1.4.

As a cross-check the summed multiplicity ratio $R_{\pi^\pm+p^\pm+K^\pm}$ is calculated. A value of 1.21 ± 0.01 is obtained in the case of Y events and 1.29 ± 0.02 in the case of Mercedes events. Both numbers are in good agreement with a direct measurement of this ratio [1].

TABLE 5 for completeness shows a comparison with measurements of other experiments. A significant excess of proton production was observed by ARGUS [15] and OPAL [16]. No direct comparison is, however, possible due to the different energies or event topologies.

[6] Note that ARIADNE employs the non-perturbative hadronization model of JETSET.

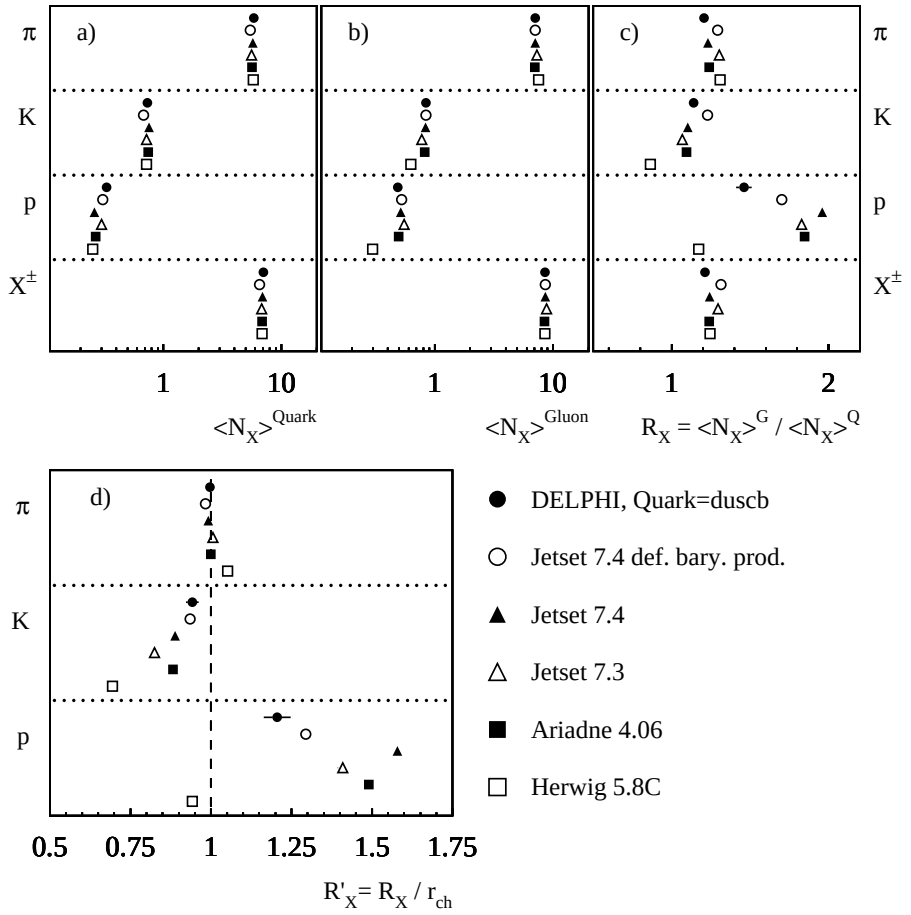

Figure 4: Mean multiplicities for identified particles in quark and gluon jets of Y events compared to different Monte Carlo models.

Systematic Errors

TABLE 6 summarizes the influences of the most important sources of systematic error for the determination of the multiplicities and their ratios. To obtain systematic errors comparable with the statistical errors, half the difference in the value obtained when a parameter is modified from its central value is quoted as the systematic uncertainty. The single errors are added quadratically. The following sources of systematic uncertainties were examined.

1. **Decays of K^0, Λ^0**
   It was examined whether the ratios of the production rates of pions, kaons and protons in quark and gluon jets are influenced by K^0_S and Λ^0 decays. These decays are reconstructed with the program MAMMOTH [17] for the data and detector simulation. At generated level of the simulation, these particles were then treated as stable particles.
2. **Secondary interactions**
   Another source of uncertainty stems from secondary produced particles from reinteractions of primary particles with the detector material. Positively charged pions and protons are produced in preference. All positive charged protons were omitted in the corresponding momentum range ($p \leq 2.7$ GeV/c) to study this effect.

Y events					
Sort	Quark	N_{Quark}	N_{Gluon}	R_X	R'_X
π	duscb	$5.852 \pm 0.036 \pm 0.071$	$7.067 \pm 0.032 \pm 0.077$	$1.208 \pm 0.009 \pm 0.020$	$0.997 \pm 0.009 \pm 0.013$
	dusc	$5.702 \pm 0.039 \pm 0.069$	$7.043 \pm 0.031 \pm 0.076$	$1.235 \pm 0.010 \pm 0.020$	$0.977 \pm 0.010 \pm 0.013$
	dus	$5.672 \pm 0.040 \pm 0.067$	$7.051 \pm 0.032 \pm 0.076$	$1.243 \pm 0.010 \pm 0.020$	$0.966 \pm 0.010 \pm 0.012$
K	duscb	$0.737 \pm 0.012 \pm 0.013$	$0.841 \pm 0.010 \pm 0.015$	$1.141 \pm 0.023 \pm 0.019$	$0.942 \pm 0.019 \pm 0.016$
	dusc	$0.692 \pm 0.013 \pm 0.013$	$0.836 \pm 0.010 \pm 0.015$	$1.208 \pm 0.026 \pm 0.020$	$0.956 \pm 0.021 \pm 0.018$
	dus	$0.637 \pm 0.013 \pm 0.012$	$0.835 \pm 0.010 \pm 0.015$	$1.310 \pm 0.031 \pm 0.022$	$1.018 \pm 0.025 \pm 0.018$
p	duscb	$0.332 \pm 0.010 \pm 0.004$	$0.485 \pm 0.009 \pm 0.008$	$1.460 \pm 0.050 \pm 0.031$	$1.205 \pm 0.041 \pm 0.025$
	dusc	$0.333 \pm 0.010 \pm 0.004$	$0.494 \pm 0.009 \pm 0.008$	$1.481 \pm 0.053 \pm 0.031$	$1.172 \pm 0.043 \pm 0.025$
	dus	$0.343 \pm 0.011 \pm 0.004$	$0.489 \pm 0.009 \pm 0.008$	$1.427 \pm 0.051 \pm 0.028$	$1.109 \pm 0.040 \pm 0.021$
$X^{\pm}$	duscb	$7.077 \pm 0.031 \pm 0.071$	$8.573 \pm 0.026 \pm 0.086$	$1.211 \pm 0.006 \pm 0.014$	1
	dusc	$6.773 \pm 0.033 \pm 0.068$	$8.560 \pm 0.026 \pm 0.086$	$1.264 \pm 0.007 \pm 0.015$	1
	dus	$6.654 \pm 0.034 \pm 0.067$	$8.559 \pm 0.026 \pm 0.086$	$1.286 \pm 0.008 \pm 0.015$	1
Mercedes events					
Sort	Quark	N_{Quark}	N_{Gluon}	R_X	R'_X
π	duscb	$6.973 \pm 0.078 \pm 0.085$	$8.962 \pm 0.133 \pm 0.096$	$1.285 \pm 0.024 \pm 0.022$	$0.998 \pm 0.023 \pm 0.012$
	dusc	$6.735 \pm 0.084 \pm 0.076$	$9.002 \pm 0.134 \pm 0.133$	$1.337 \pm 0.026 \pm 0.029$	$0.988 \pm 0.023 \pm 0.012$
	dus	$6.700 \pm 0.088 \pm 0.072$	$9.028 \pm 0.134 \pm 0.133$	$1.347 \pm 0.027 \pm 0.029$	$0.974 \pm 0.024 \pm 0.012$
K	duscb	$0.862 \pm 0.025 \pm 0.014$	$0.978 \pm 0.041 \pm 0.016$	$1.135 \pm 0.058 \pm 0.021$	$0.881 \pm 0.046 \pm 0.018$
	dusc	$0.819 \pm 0.027 \pm 0.013$	$0.982 \pm 0.042 \pm 0.011$	$1.199 \pm 0.064 \pm 0.017$	$0.886 \pm 0.049 \pm 0.016$
	dus	$0.773 \pm 0.027 \pm 0.013$	$0.981 \pm 0.042 \pm 0.011$	$1.268 \pm 0.070 \pm 0.018$	$0.917 \pm 0.052 \pm 0.017$
p	duscb	$0.401 \pm 0.022 \pm 0.006$	$0.656 \pm 0.040 \pm 0.013$	$1.635 \pm 0.134 \pm 0.049$	$1.269 \pm 0.106 \pm 0.046$
	dusc	$0.422 \pm 0.023 \pm 0.012$	$0.636 \pm 0.038 \pm 0.013$	$1.507 \pm 0.123 \pm 0.098$	$1.114 \pm 0.092 \pm 0.065$
	dus	$0.408 \pm 0.025 \pm 0.013$	$0.674 \pm 0.041 \pm 0.016$	$1.650 \pm 0.142 \pm 0.115$	$1.192 \pm 0.104 \pm 0.071$
$X^{\pm}$	duscb	$8.467 \pm 0.066 \pm 0.098$	$10.91 \pm 0.113 \pm 0.110$	$1.288 \pm 0.017 \pm 0.018$	1
	dusc	$8.085 \pm 0.071 \pm 0.097$	$10.94 \pm 0.113 \pm 0.123$	$1.353 \pm 0.018 \pm 0.025$	1
	dus	$7.942 \pm 0.074 \pm 0.089$	$10.99 \pm 0.114 \pm 0.124$	$1.384 \pm 0.019 \pm 0.024$	1

Table 3: Multiplicities of identified particles in quark and gluon jets .

3. **Particle identification**
   To take uncertainties of the particle identification into account, the results for the particle identification cuts (loose, standard, and tight) were compared.
4. **Purity correction of the jets**
   The quark sample in the normal mixture sample was varied and corrected to different flavour compositions:

Quark jets in the normal mixture	Corrected to *duscb*- quarks	Corrected to *dusc*- quarks	Corrected to *dus*- quarks
all relevant jets	x	x	
all jets in events with $\lambda_E < 1.03$	x	x	x
all jets in events with $\lambda_E < 0.73$			x

The sample containing jets with $\lambda_E < 1.03$ is b depleted and with $\lambda_E < 0.73$ is b and c depleted. λ_E is a measure of the b event probability and discussed in [5].

R'_X	Data	JT 74 def. bary.	JT 74	JT 73	AR	HW
Y Events						
R'_{π^+}	$0.997 \pm 0.009 \pm 0.013$	0.98	0.99	1.01	1.00	1.05
R'_{K^+}	$0.942 \pm 0.019 \pm 0.016$	0.94	0.89	0.82	0.88	0.69
R'_p	$1.205 \pm 0.041 \pm 0.025$	1.29	1.58	1.41	1.49	0.94
Mercedes Events						
R'_{π^+}	$0.998 \pm 0.023 \pm 0.012$	1.00	1.01	1.02	1.01	1.05
R'_{K^+}	$0.881 \pm 0.046 \pm 0.018$	0.94	0.90	0.81	0.88	0.70
R'_p	$1.269 \pm 0.106 \pm 0.046$	1.20	1.43	1.38	1.37	1.11

Table 4: Normalized multiplicity ratios R'_X (for $udscb$ quarks) compared to the predictions from the Monte Carlo simulations (JT 74 def. bary. = JETSET 7.4 PS with default baryon production, JT 74 = JETSET 7.4 PS, JT 73 = JETSET 7.3 PS, AR = ARIADNE 4.08, HW = HERWIG 5.8C).

Particle	This Paper Y	DELPHI [14]	OPAL three-jet [16]	ARGUS [15]
$\pi^\pm$	$0.997 \pm 0.009 \pm 0.013$	—	$1.016 \pm 0.0103 \pm 0.010$	1 (def.)
$K^\pm$	$0.942 \pm 0.019 \pm 0.016$	$0.930 \pm 0.040 \pm 0.020$	$0.948 \pm 0.017 \pm 0.028$	0.86 ± 0.31
$p\bar{p}$	$1.205 \pm 0.041 \pm 0.025$	$1.120 \pm 0.110 \pm 0.040$	$1.100 \pm 0.024 \pm 0.027$	1.58 ± 0.10

Table 5: R'_X from measurements of different collaborations

Furthermore the results were compared by using the CAMBRIDGE algorithm [18] instead of the DURHAM algorithm. The change of the multiplicities then is typically 2%; changes of the ratios and double ratios are much smaller. Finally a systematic error of $\lesssim 2\%$ due to track reconstruction losses as determined from the overall multiplicity measurements [19] is assumed. This error is expected to cancel in the ratios. As both systematic errors discussed below the item list apply to particles in general, those errors are not included in TABLE 6.

3.1.2 Momentum Spectra

FIGURE 5 shows the momentum spectra of identified hadrons in quark ($duscb$) and gluon jets. The momentum spectra of kaons and protons differ significantly from those of pions. Pions are produced mainly at low momentum, both in quark and gluon jets. The likely explanation is that pions are often low energy decay products of unstable particles. The Monte Carlo generators JETSET, ARIADNE, and HERWIG describe the gross features of the measured DELPHI data. The momentum distribution of kaons in gluon jets is best predicted by Ariadne. The HERWIG model shows a considerable weakness concerning the description of kaon momentum spectrum in gluon jets. The multiplicity of fast kaons is clearly underestimated. The momentum distribution of protons in gluon jets is well modelled by the JETSET and ARIADNE generators but not by the HERWIG model.

FIGURE 6 shows the ratios of the momentum spectra of identified hadrons in gluon and quark jets . This measurement is an improvement of our previous publication [14].

Y events										
Vari-able	Par-ticle	Quarks	Value	Stat. Error [%]	Summed Error with K^0, Λ [%]	Summed Error without K^0, Λ [%]	Syst. Error [%] of K^0, Λ	Sec. Int.	Part. Id.	Purity-Corr.
N_X^Q	π	duscb	5.85	0.62	-	1.21	-	1.01	0.60	0.29
		dusc	5.70	0.68	-	1.20	-	1.00	0.60	0.30
		dus	5.67	0.71	-	1.19	-	1.00	0.60	0.19
	K	duscb	0.74	1.63	-	1.77	-	0.95	1.49	0.14
		dusc	0.69	1.88	-	1.89	-	1.01	1.59	0.14
		dus	0.64	2.04	-	1.84	-	0.94	.57	0.16
	p	duscb	0.33	3.01	-	1.13	-	0.90	0.30	0.60
		dusc	0.33	3.00	-	1.12	-	0.90	0.30	0.60
		dus	0.34	3.21	-	1.09	-	0.87	.29	0.58
	$X^\pm$	duscb	7.08	0.44	-	1.01	-	1.00	0.06	0.06
		dusc	6.77	0.49	-	1.01	-	1.00	0.06	0.06
		dus	6.65	0.51	-	1.01	-	1.01	0.06	0.05
N_X^G	π	duscb	7.07	0.45	-	1.09	-	1.00	0.40	0.17
		dusc	7.04	0.44	-	1.08	-	0.99	0.38	0.17
		dus	7.05	0.45	-	1.08	-	1.01	.38	0.11
	K	duscb	0.84	1.19	-	1.75	-	0.95	1.43	0.36
		dusc	0.84	1.20	-	1.76	-	0.96	1.44	0.36
		dus	0.84	1.20	-	1.74	-	0.96	.44	0.24
	p	duscb	0.49	1.86	-	1.68	-	1.03	1.03	0.82
		dusc	0.49	1.82	-	1.64	-	1.01	1.01	0.81
		dus	0.49	1.84	-	1.57	-	1.02	.02	0.61
	$X^\pm$	duscb	8.57	0.30	-	1.01	-	1.00	0.01	0.08
		dusc	8.56	0.30	-	1.01	-	1.00	0.01	0.08
		dus	8.56	0.30	-	1.01	-	1.00	0.01	0.04
R_X	π	duscb	1.21	0.75	1.68	1.14	1.24	0.99	0.25	0.50
		dusc	1.24	0.81	1.65	1.11	1.21	0.97	0.24	0.49
		dus	1.24	0.80	1.58	1.02	1.21	0.97	.24	0.24
	K	duscb	1.14	2.02	1.65	1.63	0.26	0.96	1.31	0.09
		dusc	1.21	2.15	1.68	1.66	0.25	0.99	1.32	0.08
		dus	1.31	2.37	1.68	1.64	0.31	0.99	1.30	0.08
	p	duscb	1.46	3.42	2.13	2.11	0.27	1.03	0.96	1.58
		dusc	1.48	3.58	2.08	2.06	0.27	1.01	1.01	1.49
		dus	1.43	3.57	1.99	1.97	0.28	0.98	0.98	1.40
	$X^\pm$	duscb	1.21	0.50	1.19	0.99	0.66	0.99	0.08	0.00
		dusc	1.26	0.55	1.21	1.03	0.63	1.03	0.08	0.00
		dus	1.29	0.62	1.19	1.01	0.62	1.01	0.08	0.00
R'_X	π	duscb	1.00	0.90	1.27	1.12	0.60	1.00	0.30	0.40
		dusc	0.98	1.02	1.30	1.14	0.61	1.02	0.31	0.41
		dus	0.97	1.04	1.26	1.19	0.62	1.04	0.31	0.21
	K	duscb	0.94	2.02	1.73	1.51	0.85	0.96	1.17	0.11
		dusc	0.96	2.20	1.89	1.64	0.94	1.05	1.26	0.10
		dus	1.02	2.46	1.77	1.54	0.88	0.98	1.18	0.10
	p	duscb	1.21	3.40	2.10	2.08	0.33	1.00	0.91	1.58
		dusc	1.17	3.67	2.10	2.07	0.34	1.02	0.94	1.54
		dus	1.11	3.61	1.94	1.90	0.36	0.99	0.90	1.35

Table 6: Systematic errors for N_X^Q, N_X^G, R_X and R'_X in Y events. Here X denotes the particle species π, K, p or all charged particles.

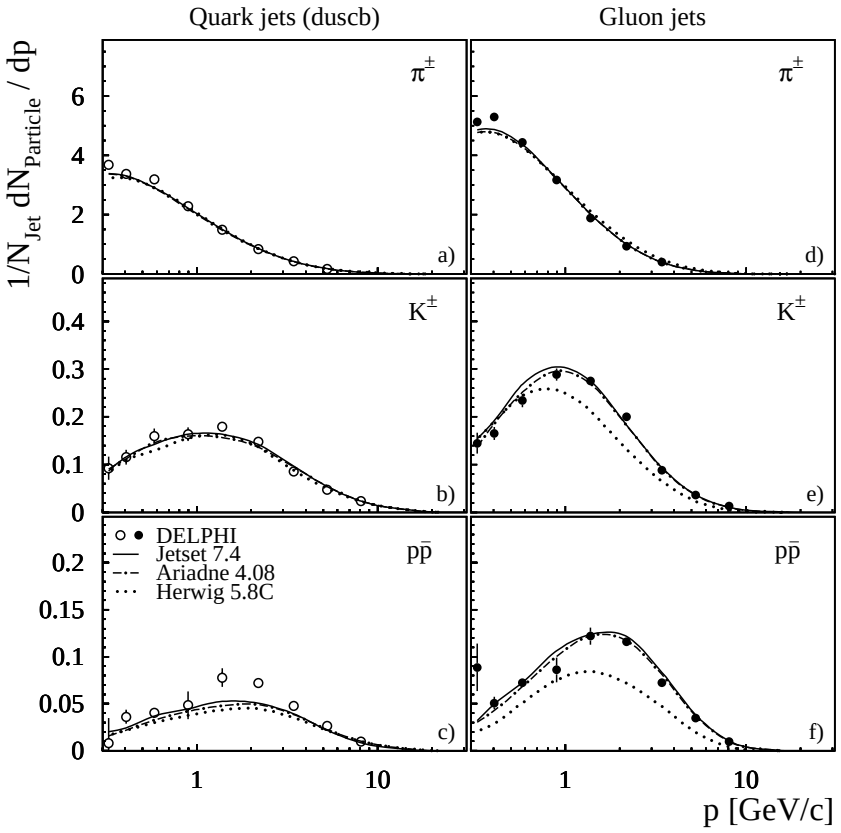

Figure 5: Momentum spectra of identified hadrons in quark and gluon jets a)-c) spectra of pions, kaons, and protons in quark jets; d)-f) corresponding spectra for gluon jets in events with Y topology; The predictions of the generator models JETSET, ARIADNE und HERWIG are drawn as lines.

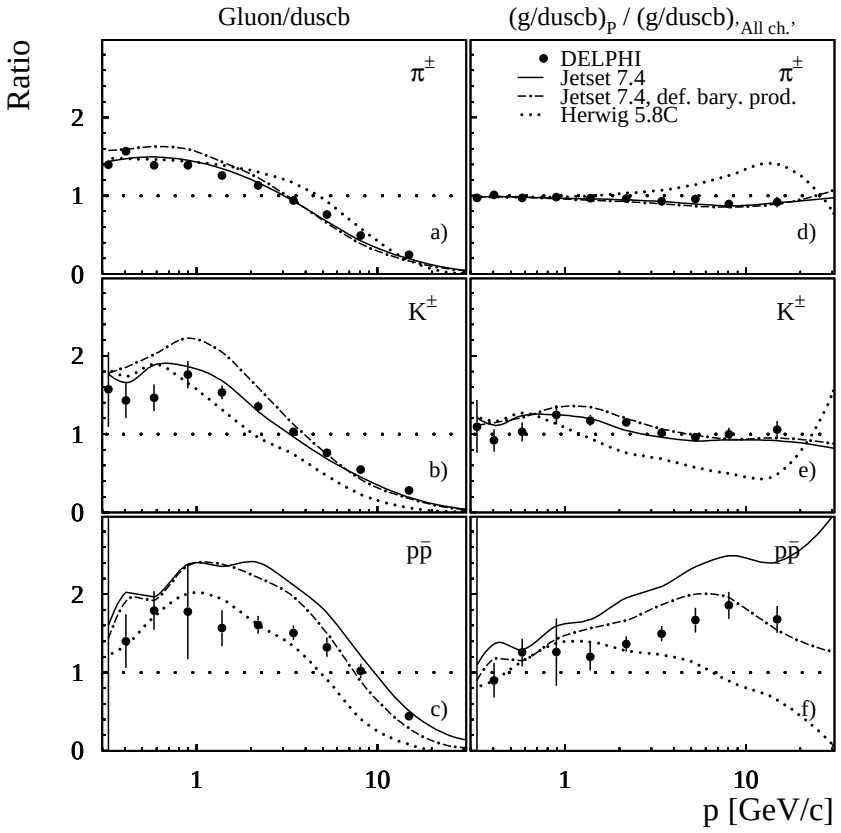

Figure 6: Ratios of the momentum spectra of identified hadrons in gluon and quark jets of Y events; a)-c) ratios of the spectra of pions, kaons, and protons in gluon jets to those in quark jets; d)-f) corresponding spectra normalized to the ratio gluon/quark for all charged particles; The predictions of the generator models JETSET, JETSET with default baryon production model and HERWIG are drawn as lines.

More low energy particles are produced in gluon jets than in quark jets for all kinds of particles. At high particle momenta this structure is inverted. FIGURE 6(d,e,f) shows the corresponding ratios of the momentum spectra of FIGURE 6(a,b,c) normalized to the momentum spectra of all charged particles in gluon and quark jets .

FIGURE 6(f) indicates that the proton enhancement in gluon jets is bigger than that for all charged particles. The overestimate of the proton production ratio by JETSET or ARIADNE (not shown) presumably is due to an extra suppression of baryon production at the end of the string (i.e. for quark jets). A much better description is obtained using the default baryon production model without this extra suppression.

It should be mentioned, however, that from these normalized ratios as a function of momentum, no direct conclusions concerning the ratios of the multiplicities can be drawn because the shapes of the momentum spectra of kaons and protons differ significantly from those of pions which dominate the all charged particle sample.

3.1.3 Rapidity

FIGURE 7 shows the rapidity spectra of identified hadrons in quark and gluon jets and FIGURE 8 shows the corresponding ratios. For all particles there are in the plateau, i.e. at low η, 1.6-2 times more particles in gluon jets indicating the higher colour charge of the gluon. At high η, i.e. in the range of the leading particle only few kaons and protons are observed in gluon jets.

3.1.4 ξ-Spectra

FIGURE 9 shows the $\xi_p^{'}$ spectra of identified hadrons in quark and gluon jets . The JETSET and ARIADNE (not shown) models provide a reasonable description over a wide range of the $\xi_p^{'}$ spectrum. The maximum height is different for quark and gluon jets which indicates different particle rates. The point of intersection of the $\xi_p^{'}$ distributions of quark and gluon jets for pions and kaons is approximately the same, $\xi_p^{'(s)} \sim 0.75$. For protons the crossing point between the quark and gluon distributions is shifted to higher momentum at $\xi_p^{'(s)} \sim 0.32$. Proton production is enhanced in gluon jets, but preferentially at high momenta. This is seen more clearly in FIGURE 10 which shows the normalized ratio $R_p^{'}(\xi_p^{'})$. It is observed that this ratio is unity within error at very small $\xi_p^{'}$ (highest momenta) and close to unity also at large $\xi_p^{'}$ (small momenta). A strong deviation from unity is, however, visible in the intermediate $\xi_p^{'}$ region ($0.3 \leq \xi_p^{'} \leq 0.8$).

A surplus of baryon production in gluon jets and the observed kinematical properties can be qualitatively understood if baryons are directly produced from coloured partons or equivalently from a colour string. In a parton shower colour conservation leads to the so-called preconfinement property, that is a local compensation of colour charge in space. Alternatively the produced colour charges can always be ordered to form continuous chains or strings in space time. These strings appear naturally in the Lund fragmentation model [7] and in the progenitor model of Feynman and Field [20]. A colour string ends at the primary quarks produced in the underlying hard scattering but is spanned over the corresponding gluons. Hadron production now can be assumed to proceed via a pair-creation of a quark-anti-quark (or diquark-anti-diquark) pair and a corresponding string break-up. A single break-up in the vicinity of a primary quark will produce a leading hadron, whereas close to the gluon in the centre of the string at least two breaks are needed before a hadron is formed. To produce a baryon a production of a diquark-anti-diquark pair is compelling. Now it should be noted that in the centre of a string (i.e.

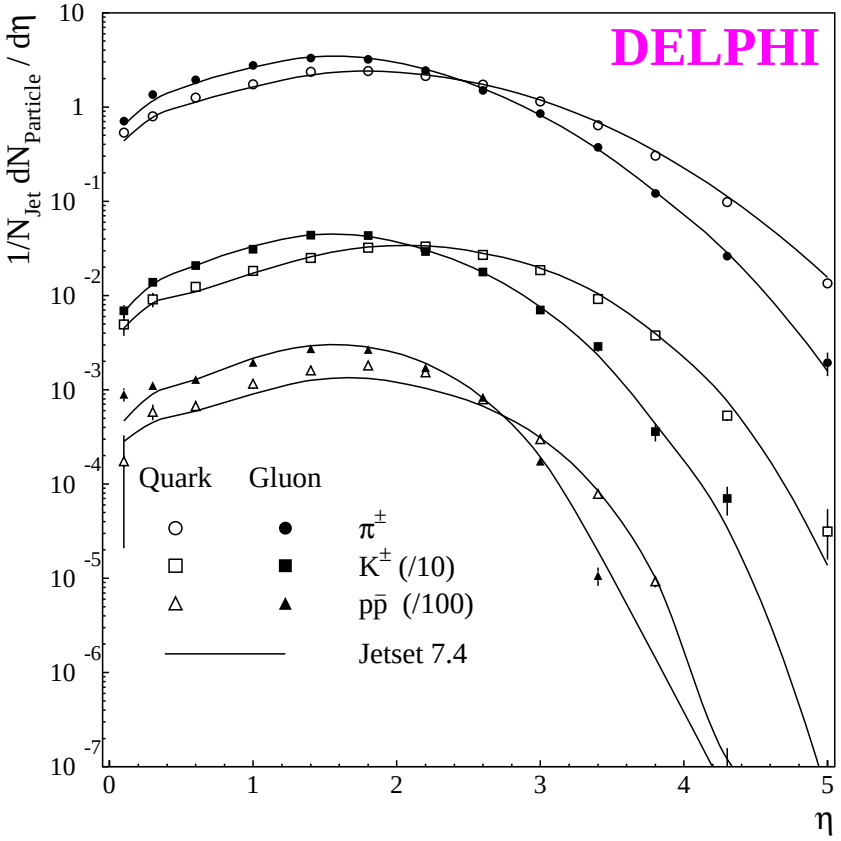

Figure 7: Rapidity spectra of identified hadrons in quark and gluon jets compared to JETSET in events with Y topology

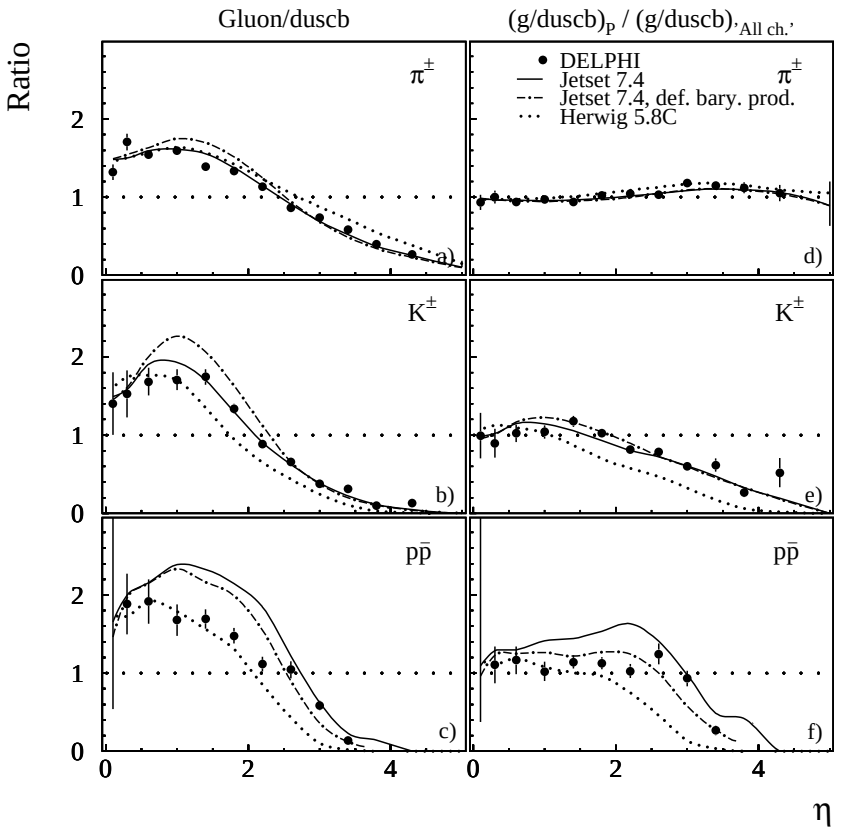

Figure 8: Ratios of the rapidity spectra of identified hadrons in gluon and quark jets from Y events; a)-c) ratios of the spectra of pions, kaons, and protons in gluon jets to those in quark jets ; d)-f) corresponding spectra normalized to the ratio gluon/quark for all charged particles; The predictions of the generator models JETSET, JETSET with the default baryon production model, and HERWIG are drawn as lines.

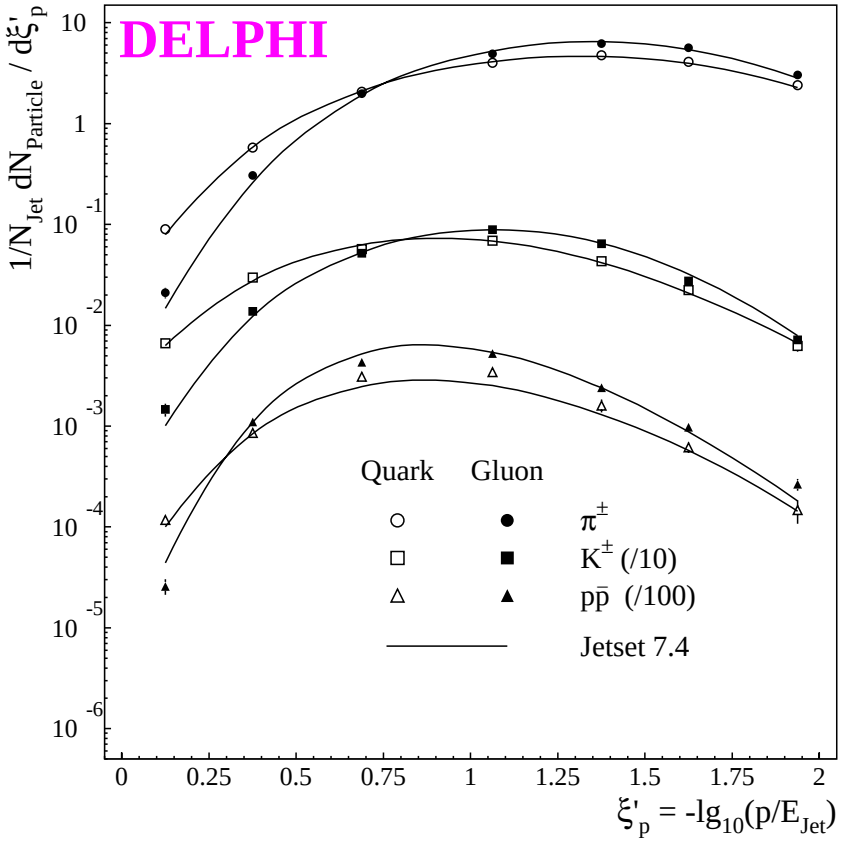

Figure 9: $\xi_p^{'}$ spectra of identified hadrons in quark and gluon jets compared to JETSET in events with Y topology

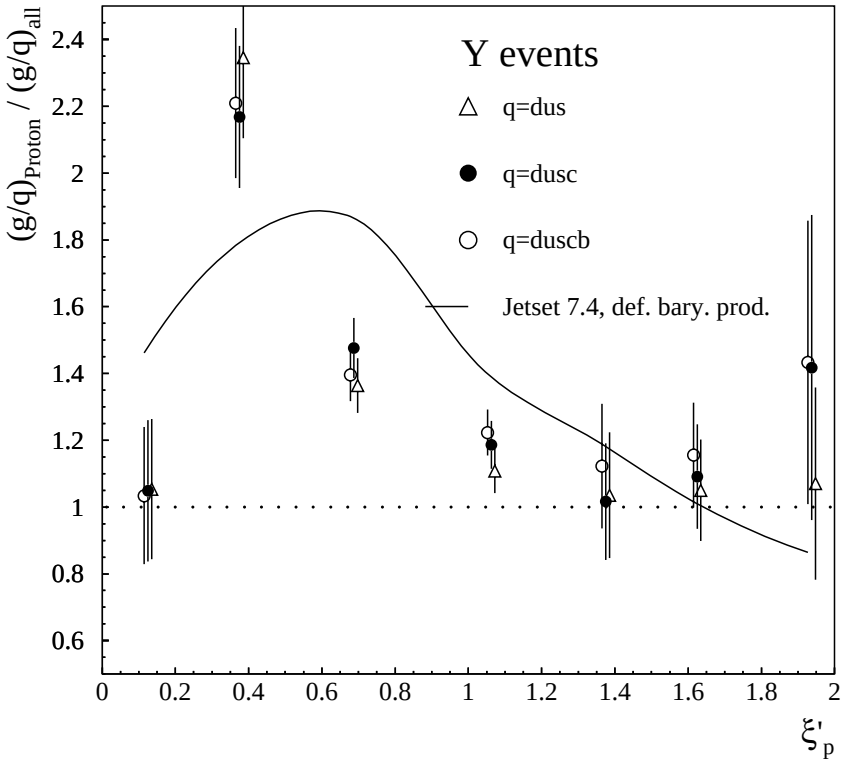

Figure 10: Normalized ratio $R_p^{'} = R_p/R_{X^{\pm}}$ for different compositions of the quark event sample.

in the vicinity of the gluon) more possibilities exist which lead to baryon formation. A primary diquark-anti-diquark break up as well as a secondary one following a primary quark-anti-quark creation lead to baryon production (see FIGURE 11).

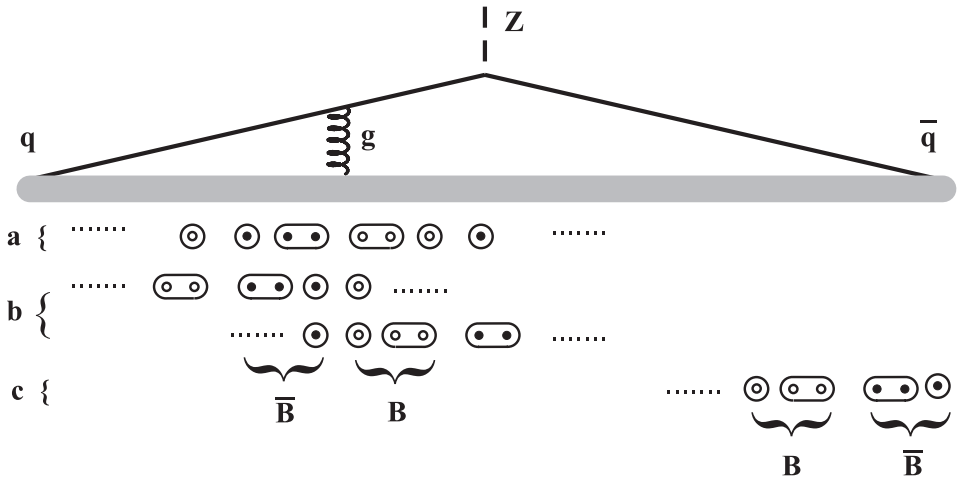

Figure 11: Different possibilities of baryon production in strings. The single points denote quarks and the double points diquarks. Open points stand for quarks and filled points for anti-quarks. Line a} illustrates a primary splitting into diquark-anti-diquark in the center of the string. Line b} shows the possibilities for secondary diquark production. Line c} shows a diquark-anti-diquark splitting at a string end.

The latter process (marked b} in FIGURE 11) may happen in both remaining strings similarly to both original endpoints of the string (see FIGURE 11 c}). The first production mechanism (marked a} in FIGURE 11) is missing at the string end and leads to the excess pf gluon compared to quark jets. Here it is likely that two leading baryons are produced which take a large fraction of the gluon energy. Thus it is expected that the excess of baryon production centers at comparably large scaled momentum which is indeed observed (see FIGURE 10). At small momentum, i.e. in the momentum range where baryons from the inner part of the string between the jets are expected to contribute, the relative portion of baryon production in quark and gluon jets is approximately equal.

Although the above discussion centers around the string model it is based on quite general topological properties and is a strong indication that baryon production, and presumably also meson production, happens directly from coloured objects and an intermediate step of colour and baryon number neutral objects is avoided. In particular this is also indicated by the failure of the HERWIG model to describe the surplus of proton production observed in the data.

In detail the above described mechanism will be complicated by the abundant production of resonant baryons [21]-[22] or equivalently the so-called popcorn-mechanism [7]. Further support to this interpretation comes from the observed strong energy dependence of the surplus of baryon production (compare the ARGUS measurement at $\sqrt{s} \simeq 10$GeV to this result in TABLE 5). The surplus of baryons in gluon jets is due to the leading baryons. As energy and thus the multiplicity ratio in gluon to quark jets increases [1] this excess is less and less important in the double ratio $R_p^{'}$. The Lund model qualitatively describes the decrease of $R_p^{'}$ shown in TABLE 5.

FIGURE 12 shows the maxima of the ξ_p distributions fitted with a simple Gaussian in dependence of the scale $\kappa = E_{jet} \cdot \sin\theta_{min}/2$ with θ_{min} being the angle with respect to the

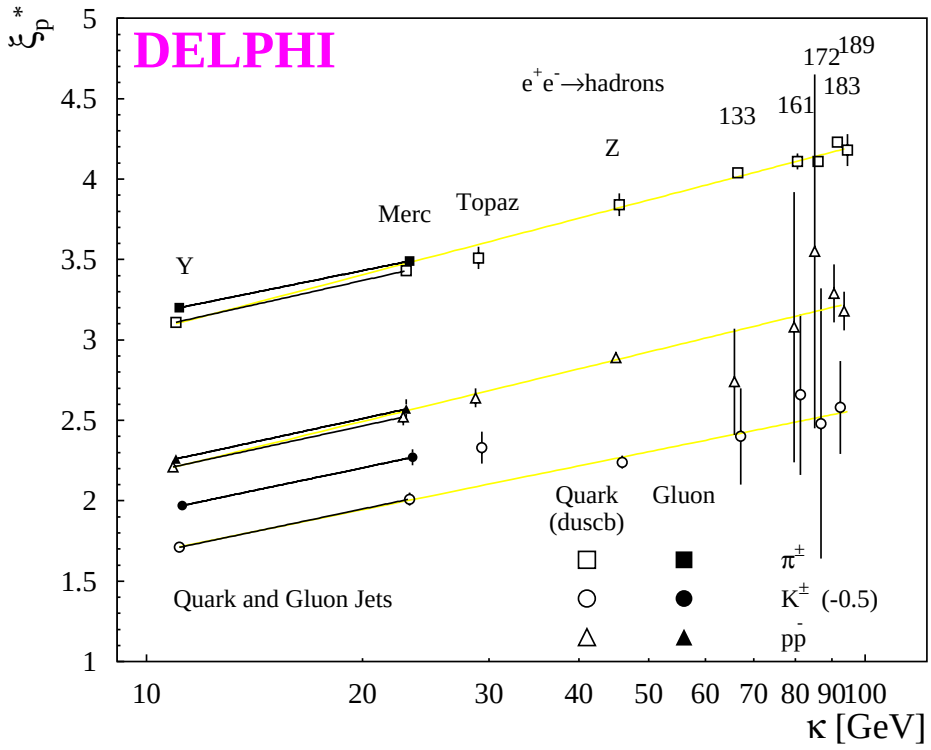

Figure 12: Fitted maxima of the ξ_p spectra from Y and Mercedes events. Here $\kappa = E_{jet} \sin \frac{\theta_1}{2}$ denotes the underlying jet scale. Observe the offset of 0.5 units for the ξ_p^* values for the $K^{\pm}$.

closest jet, here $\theta_{min} = \theta_1$ (for a detailed discussion of jet scales see [13]). The fit results are given in TABLE 7. The maxima of the ξ_p distributions for protons and kaons for quark jets are shifted to smaller values (i.e. higher momenta) compared to pions as has been observed previously. It is clearly observed that the maximum is shifted to smaller ξ_p for K's in quark compared to gluon jets. To a lesser extent this is also observed for π's and p's. In MLLA/LPHD the maxima of the ξ_p spectra for gluons and quarks are expected to be almost identical [13,23]. A natural explanation for the observed difference especially for K's is the leading particle effect.

For all particles the ξ_p^* values are bigger for Mercedes compared to Y events, i.e. a scale evolution of the ξ_p spectra is observed (see FIGURE 12 and TABLE 7). Assuming a general linear increase of ξ_p^* with the logarithm of the scale κ, i.e.

$$f(\xi_p^*) = a + b \ln(\kappa)$$

Y events		
particle	ξ_p^*	
	quark	gluon
π	3.11 ± 0.01	3.20 ± 0.00
K	2.21 ± 0.02	2.47 ± 0.01
p	2.21 ± 0.02	2.26 ± 0.01
$X^{\pm}$	2.93 ± 0.01	3.05 ± 0.00

Mercedes events		
particle	ξ_p^*	
	quark	gluon
π	3.43 ± 0.03	3.49 ± 0.02
K	2.51 ± 0.04	2.77 ± 0.05
p	2.52 ± 0.05	2.57 ± 0.06
$X^{\pm}$	3.24 ± 0.02	3.35 ± 0.02

Table 7: Maxima of the ξ_p distributions

the quark jet measurements extrapolate reasonably well to the measurements performed by TOPAZ [24], for overall Z events [25], and for high energy events [26]. The TASSO measurements at low energy [24] are omitted from the plot as they overlap with the DELPHI quark and gluon jet results. Also the quark composition is largely different for those low energy data. The grey lines in FIGURE 12 indicate fits including the TOPAZ, Z, and higher energy data.

It is further remarkable, that contrary to the predictions of the LPHD model, the peak values of the ξ_p distributions for kaons and protons in quark jets are almost equal (ξ_p^* values for the $K^{\pm}$ in FIGURE 12 are shifted by 0.5 units to avoid overlaps with the proton results.). This observation contradicts the predictions of the LPHD concept that the positions of the maxima of the ξ_p distributions are proportional to the logarithm of the mass of the corresponding particle. It has already been shown (see e.g. [27]) that mesons and baryons show a behaviour which differs from this simple expectation. This is a consequence of heavy particle decays and of the partially different masses of the decay particles in (predominantly baryon) decays. This statement is qualitatively confirmed by this analysis.

3.2 Resonances

To measure resonances, the following procedure was applied. Firstly, single particles were tagged as kaons or pions and the energy of the particles was recalculated assuming the correct mass of the tagged particle . Secondly, any two particles with opposite sign (KK in the case of the $\phi(1020)$ and $K\pi$ for the $K^*(892)^0$) were combined. It was further required that at least one of the particles was *standard* tagged in the case of $\phi(1020)$ and that both were *standard* tagged for the $K^*(892)^0$. Then the four-momenta of the two particles were added to form a quasi particle and the invariant mass was calculated. In the last step the particle was assigned to a jet according to the minimal angle in space.

	$\phi(1020)$		$K^*(892)^0$	
	Gluon	**Normal Mixture**	**Gluon**	**Normal Mixture**
$N_{observed}/N_{jet}$	0.0032 ± 0.0006	0.0037 ± 0.0003	0.022 ± 0.003	0.019 ± 0.001
$\chi^2_{n.d.f.}$	1.2	1.7	0.6	1.4
$\chi^2_{n.d.f.,back.}$	0.7	1.1	0.8	2.0
Signal/Back.	1/1.1	1/1.1	1/12.4	1/13.9

Table 8: Results of the fits of the $\phi(1020)$ and $K^*(892)^0$ resonances in tagged gluon jets and normal mixture jets

The fit of the invariant mass spectra shown in FIGURE 13 and FIGURE 14 was performed using a Breit-Wigner with , fixed to the nominal values [28] plus a smooth background, $F(m) = BW(m) + F_{back}(m)$:

$$BW(m) = N \frac{,^2}{4(m-m_0)^2 + ,^2}$$

$$F_{back}(m) = \frac{a_1 \cdot (m - M_{threshold})^{a_2}}{\exp\{A(m)\}} .$$

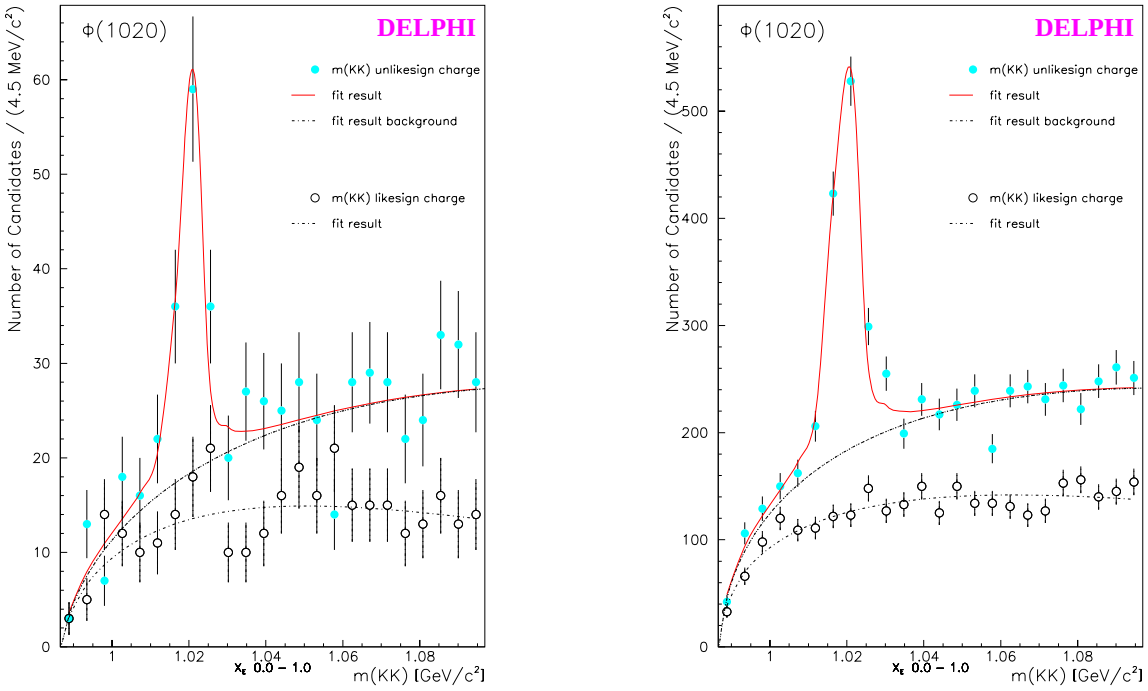

Figure 13: $\phi(1020)$ resonance in gluon (left) and normal mixture (right) jets from Y events.

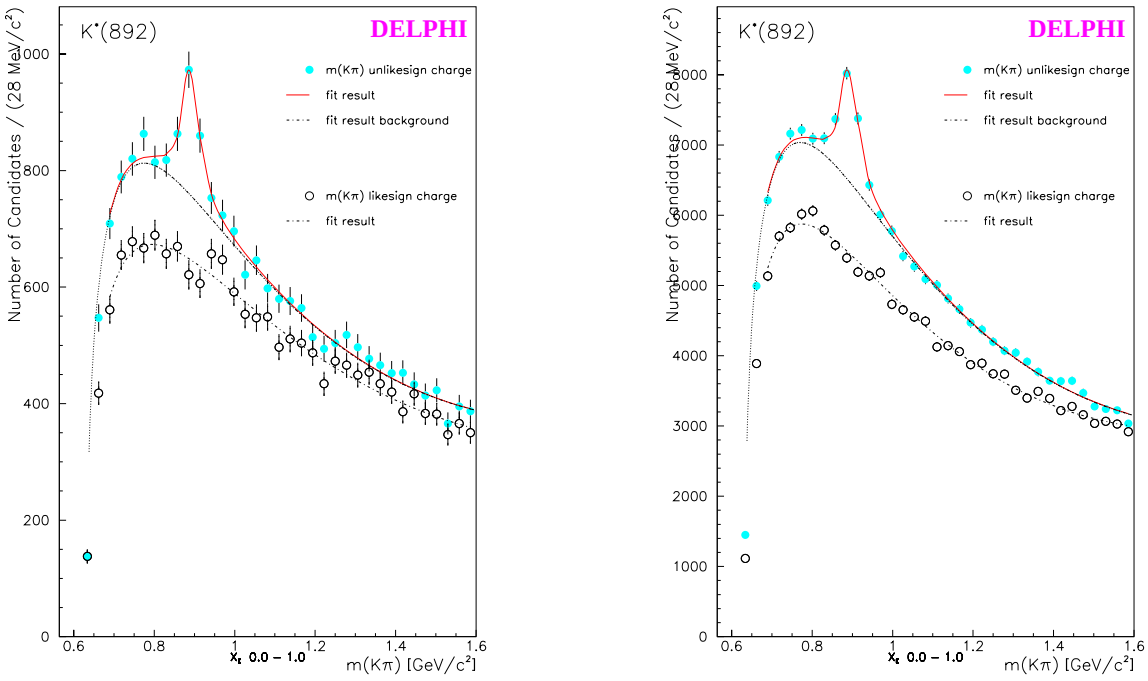

Figure 14: $K^*(892)^0$ resonance in gluon (left) and normal mixture (right) jets from Y events.

Here m_0 is the mass of the resonance, N is a normalization factor and $A(m) = \sum_{i=3}^{k} a_i (m - M_{threshold})^{i-2}$ ($k = 3$ for $\phi(1020)$, $k = 4$ for $K^*(892)^0$). The fits are indicated in FIGURE 13 and FIGURE 14 by solid lines. The results of the fits are presented in TABLE 8. The fitted masses are fully consistent with the PDG expectation.

The ansatz of $F_{back}(m)$ describes the combinatorial background which results from likesign charged kaons and pions well (open points and dashed lines). The quoted numbers of $\phi(1020)$ and $K^*(892)^0$ candidates as well as the signal to background ratio were determined by integrating the functions $F(m)$ and $F_{back}(m)$ in the range $(m \pm 2.5 \cdot ,)$. They are not corrected for detector acceptance as in the gluon/quark ratio the acceptance correction as well as systematic errors are expected to cancel. Remaining errors are expected to be negligible with respect to the statistical error. The correction to pure quarks and gluons is, however, applied. The final ratio yields:

$$R_\phi = \frac{N_g}{N_q} = 0.7 \pm 0.3 \quad \text{for the } \phi(1020) \text{ and}$$

$$R_{K^{*0}} = \frac{N_g}{N_q} = 1.7 \pm 0.5 \quad \text{for the } K^*(892)^0 .$$

This may be compared to the expectation of $R_\phi = 0.90$ (0.60) and $R_{K^{*0}} = 1.0$ (0.96) for JETSET and HERWIG, respectively. Thus no excess of isoscalar $\phi(1020)$ production is observed in (isoscalar) gluon jets. This result does not change within errors if only $\phi(1020)$ candidates with $x_p > 0.07$ are used, to take into account that soft particles may not be uniquely assignable to individual jets.

4 Summary and Conclusion

Based on a sample of about 2.2 million hadronic Z decays collected by the DELPHI detector at LEP, the production of identified particles in jets initiated by gluons or by quarks, was analysed in order to search for possible differences.

As observed for inclusive charged particles, the production spectrum of identified particles was found to be softer in gluon jets compared to quark jets, with a higher total multiplicity. The normalized multiplicity ratio (R') for protons in Y events was measured to be:

$$R'_p = \frac{R_p}{r_{ch}} = \frac{(N_p/N_{ch.})_g}{(N_p/N_{ch.})_q} = 1.205 \pm 0.041_{stat.} \pm 0.025_{sys.}.$$

HERWIG underestimates both the kaon and the proton production in gluon jets.

This surplus of baryon production in gluon jets indicates that baryons are produced directly from coloured partons or from strings. This interpretation is supported by the scaled energy dependence of the proton excess and by the evolution of this excess with energy scale.

Furthermore the ξ_p and η distributions were measured and agreement with the JETSET and ARIADNE models was found. HERWIG underestimates both the kaon and the proton production in gluon jets. The maxima of the ξ distributions of quark jets, ξ_p^*, extrapolate well with the scale κ to those obtained from all events at different centre-of-mass energies. For kaons the maximum is shifted to smaller ξ_p^* compared to gluon jets presumably because of a leading particle effect.

The $\phi(1020)$ and the $K^*(892)^0$ resonances were measured for the first time in identified quark and gluon jets demonstrating the powerful particle identification capabilities of

DELPHI. The ratio gluon/quark of the isoscalar $\phi(1020)$ resonance was measured to be:

$$R_\phi = \frac{N_g}{N_q} = 0.7 \pm 0.3,$$

in agreement with the model predictions. No excess of ϕ production is observed.

Acknowledgements

We thank T. Sjöstrand for useful and illuminating discussions, especially for pointing out the possible explanation of the excess of baryon production in gluon jets.
We are greatly indebted to our technical collaborators, to the members of the CERN-SL Division for the excellent performance of the LEP collider, and to the funding agencies for their support in building and operating the DELPHI detector.
We acknowledge in particular the support of
Austrian Federal Ministry of Science and Traffics, GZ 616.364/2-III/2a/98,
FNRS–FWO, Belgium,
FINEP, CNPq, CAPES, FUJB and FAPERJ, Brazil,
Czech Ministry of Industry and Trade, GA CR 202/96/0450 and GA AVCR A1010521,
Danish Natural Research Council,
Commission of the European Communities (DG XII),
Direction des Sciences de la Matière, CEA, France,
Bundesministerium für Bildung, Wissenschaft, Forschung und Technologie, Germany,
General Secretariat for Research and Technology, Greece,
National Science Foundation (NWO) and Foundation for Research on Matter (FOM), The Netherlands,
Norwegian Research Council,
State Committee for Scientific Research, Poland, 2P03B06015, 2P03B1116 and SPUB/P03/178/98,
JNICT–Junta Nacional de Investigação Científica e Tecnológica, Portugal,
Vedecka grantova agentura MS SR, Slovakia, Nr. 95/5195/134,
Ministry of Science and Technology of the Republic of Slovenia,
CICYT, Spain, AEN96–1661 and AEN96-1681,
The Swedish Natural Science Research Council,
Particle Physics and Astronomy Research Council, UK,
Department of Energy, USA, DE–FG02–94ER40817.

References

[1] DELPHI Collab., P. Abreu et al., Phys. Lett. **B449** (1999) 383.
[2] Yu.L. Dokshitzer, V.A. Khoze, A.H. Mueller, S.I. Troyan, *Basics of perturbative QCD*, Editions Frontieres, 1991.
[3] DELPHI Collab., P. Abreu et al., Nucl. Instr. Meth. **A378** (1996) 57;
DELPHI Collab,. P. Abreu et al., Nucl. Instr. Meth. **A303** (1991) 233.
[4] DELPHI Collab., P. Abreu et al., Eur. Phys. J. **C4** (1998) 1.
[5] Thesis O. Klapp, BUGh WUPPERTAL **WUB-DIS 99-16**;
Thesis P. Langefeld, BUGh WUPPERTAL **WUB-DIS 99-3**.
[6] DELPHI Coll., P. Abreu et al., *DELPHI event generation and detector simulation*, DELPHI 89-67 PROG-142.
[7] T. Sjöstrand, Comp. Phys. Comm. **39** (1986) 346;
T. Sjöstrand, M. Bengtsson, Comp. Phys. Comm. **43** (1987) 367;
T. Sjöstrand, *JETSET 7.3 Program and Manual*, CERN-TH 6488/92.
[8] DELPHI Collab., P. Abreu et al., Z. Phys. **C73** (1996) 11.
[9] L. Loennblad, *ARIADNE 4.4 Program and Manual*, Comp. Phys. Comm. **71** (1992) 15.
[10] G. Marchesini und B.R. Webber, Nucl. Phys. **B 283** (1984) 1;
B.R. Webber, Nucl. Phys. **B 283** (1984) 492.
[11] S. Catani, Yu.L. Dokshitzer, M. Olsson, G. Turnrock, B.R. Webber, Phys. Lett. **B269** (1991) 432;
S. Bethke, Z. Kunszt, D.E. Soper, W.J. Stirling, Nuclear Physics **B370** (1992) 310.
[12] DELPHI Collab., P. Abreu et al., Z. Phys. **70** (1996) 179 (and references therein).
[13] DELPHI Collab., P. Abreu et al., CERN-EP/99-144, accepted by Eur. Phys. J. **C**.
[14] DELPHI Collab., P. Abreu et al., Phys. Lett. **B401** (1997) 118.
[15] ARGUS Collab., H. Albrecht et al. Phys. Rev. **276** (1996), 223.
[16] OPAL Collab., G. Alexander et al., Eur. Phys. J. **C8** (1999) 2241.
[17] DELPHI Collab., P. Abreu et al., Nucl. Instr. and Meth. **A378** (1996) 57.
[18] Yu.L. Dokshitzer, G. Leder, S. Moretti and B. Webber, JHEP**08**, (1997) 1;
S. Bentvelsen and I. Meyer, Eur. Phys. J. **C4** (1998) 623.
[19] DELPHI Collab., P. Abreu et al., Phys. Lett. **B372** (1996) 172.
[20] R.D. Field and R.P. Feynman, Nucl. Phys. **B136** (1978), 1.
[21] OPAL Collab., G. Alexander et al., Z. Phys. **C73** (1997), 569;
DELPHI Collab., P. Abreu et al., *Inclusive* Σ^- *and* $\Lambda(1520)$ *production in hadronic Z decays*, CERN-EP-2000-009, submitted to Phys. Lett. B.
[22] DELPHI Collab., P. Abreu et al., Phys. Lett. **B361** (1995) 207;
OPAL Collab., G. Alexander et al., Phys. Lett. **B358** (1995) 162.
[23] C.P. Fong, B.R. Webber, Phys. Lett. **B229** (1989) 289;
R.K. Ellis, W.J. Sterling, B.R. Webber, *QCD and Collider Physics*, Cambridge University Press, ISBN 0 521 58189 3 (1996).
[24] N.C. Brümmer, Z. Phys. **C66** (1995) 367.
[25] DELPHI Collab., P. Abreu et al., Eur. Phys. J. **C 5** (1998) 585.
[26] DELPHI Collab., P. Abreu et al., *Charged and Identified Particles from the hadronic decay of W bosons and in* $e^+e^- \to q\bar{q}$ *from 130 to 200 GeV*, CERN-EP-2000-023, submitted to Eur. Phys. J. C.
[27] DELPHI Collab., P. Abreu et al., Nucl. Phys. **B444** (1995) 3;
[28] Particle Data Group, Eur. Phys. J. **C 3** (1998) 1.